



# 1 **A unified Hapke-HSR + MARMIT-2 soil radiative transfer model** 2 **for reflectance simulation under varying moisture conditions**

3 Anxin Ding<sup>1,2,3</sup>, Han Ma<sup>4</sup>, Shunlin Liang<sup>4\*</sup>, Ziti Jiao<sup>5,6</sup>, Alexander A.Kokhanovsky<sup>7</sup>, Hanyu Shi<sup>8</sup>, Rui  
4 Xie<sup>9</sup>

5 <sup>1</sup>Key Laboratory of Humid Subtropical Eco-Geographical Process (Ministry of Education), Fujian Normal University,  
6 Fuzhou 350000, China

7 <sup>2</sup>School of Geographical Sciences, School of Carbon Neutrality Future Technology, Fujian Normal University, Fuzhou  
8 350000, China

9 <sup>3</sup>Anhui Academic Society for Spatial Remote Sensing, Hefei 230009, China

10 <sup>4</sup>Jockey Club STEM Laboratory of Quantitative Remote Sensing, Department of Geography, University of Hong Kong,  
11 Hong Kong 999077, China

12 <sup>5</sup>State Key Laboratory of Remote Sensing Science, Beijing Normal University, Beijing 100875, China

13 <sup>6</sup>Faculty of Geographical Science, Institute of Remote Sensing Science and Engineering, Beijing Normal University, Beijing  
14 100875, China

15 <sup>7</sup>German Research Center for Geosciences, Telegrafenberg, 14473 Potsdam, Germany

16 <sup>8</sup>School of Geospatial Artificial Intelligence, East China Normal University, Shanghai 200241, China.

17 <sup>9</sup>International Institute for Earth System Sciences, and School of Geography and Ocean Science, Nanjing University,  
18 Nanjing 210023, China.

19

20 *Correspondence to: Shunlin Liang (shunlin@hku.hk)*

21 **Abstract.** Soil radiative transfer models (RTMs) provide a physical basis for interpreting surface reflectance and  
22 retrieving land-surface parameters. However, most existing soil RTMs represent either the spectral-directional  
23 scattering behavior of dry soils or the moisture-induced absorption effects of wet soils, and a physically consistent  
24 formulation capable of jointly describing both processes remains limited. In this study, we develop a unified soil  
25 RTM by refining the Hapke-based hyperspectral reflectance model (Hapke-HSR) using dry soil reflectance and  
26 dynamically coupling it with the improved multilayer RTM of soil reflectance (MARMIT-2). The proposed Hapke-  
27 HSR + MARMIT-2 model explicitly represents the interaction between particle scattering and moisture-dependent  
28 absorption and refraction processes, enabling joint spectral-directional simulation of soil reflectance under varying  
29 soil moisture conditions. The model is systematically evaluated using eight independent soil spectral databases  
30 spanning a wide range of textures and moisture levels. Results show that the Hapke-HSR + MARMIT-2 model  
31 consistently improves simulation accuracy and stability relative to the individual Hapke-HSR and MARMIT-2  
32 models, with particularly pronounced gains at high soil moisture regimes ( $SMC \geq 30\%$ ). Across all datasets, the  
33 proposed model achieves higher performance ( $R^2 = 0.993$ ,  $RMSE = 0.007$ ) than MARMIT-2 ( $R^2 = 0.983$ ,  $RMSE =$   
34  $0.012$ ) and Hapke-HSR ( $R^2 = 0.909$ ,  $RMSE = 0.028$ ). The proposed framework provides a physically interpretable  
35 and extensible basis for soil reflectance modeling and offers a robust foundation for future developments in multi-  
36 angular hyperspectral remote sensing and land-surface parameter inversion.

37 **Keywords:** Soil radiative transfer model, soil reflectance, Hapke-HSR model, MARMIT-2 model, soil moisture  
38 content

## 39 **1 Introduction**

40 Soils are fundamental components of the Earth's surface system and play a critical role in agricultural productivity,  
41 ecosystem functioning, and hydrological processes (Fan et al., 2025; Rizzo et al., 2023; Shoshany et al., 2022). Soil  
42 reflectance is governed by a range of physical properties, including soil moisture content (SMC), particle size, and surface  
43 roughness, which jointly regulate the scattering and absorption of solar radiation (Gholami et al., 2018; Labaree et al., 2019;  
44 Nolin and Liang, 2008; Sheng et al., 2024). Among these factors, SMC is one of the most influential and dynamic variables,



45 exerting a dominant control on soil spectral behavior, particularly in the shortwave infrared region where water absorption  
 46 features are pronounced (Babliet et al., 2019; Jiang and Fang, 2019; Xu et al., 2025). Because soil reflectance constitutes a  
 47 fundamental component of optical remote sensing signals, a physically consistent soil radiative transfer model is essential for  
 48 reliably linking observed reflectance to soil and vegetation parameters and for supporting the inversion of land-surface  
 49 biophysical variables (Gao et al., 2024; Lei et al., 2025; Yang et al., 2025).

50 Soil radiative transfer models (RTMs) describe the absorption, scattering, and transmission of solar radiation within soil  
 51 media and provide a physically based framework for linking surface reflectance to soil properties (Bach and Mauser, 1994;  
 52 Jacquemoud, 1992; Liang and Townshend, 1996a, b; Sadeghi et al., 2007). Owing to their explicit physical formulation,  
 53 RTMs have become a fundamental tool for the inversion of soil-related parameters from optical remote sensing observations.  
 54 Moreover, soil reflectance constitutes a key background component of vegetation canopies and directly affects the accuracy  
 55 of vegetation radiative transfer models and the retrieval of biophysical vegetation variables (Ni and Li, 2000; Ma et al.,  
 56 2017a, b; Yang, 2022; Zeng et al., 2021). Despite substantial progress, important limitations remain in current soil RTMs.  
 57 Many widely used models, including the multilayer radiative transfer model of soil reflectance (MARMIT) (Babliet et al.,  
 58 2019) and the brightness-shape-moisture (BSM) model (Verhoef et al., 2018), rely on simplified assumptions of soil  
 59 reflectance behavior and do not fully capture the combined spectral variability and moisture-dependent effects of natural  
 60 soils (Jiang and Fang, 2019; Yang, 2022). Consequently, the development of physically consistent soil RTMs that can jointly  
 61 represent spectral behavior and moisture-driven processes remains a critical requirement for reliable surface radiative  
 62 transfer modeling and parameter inversion (Cheng et al., 2022; Jiang et al., 2023; Li et al., 2021; Verhoef et al., 2007).

63 **Table 1.** Summary of the strengths and limitations of existing soil radiative transfer models.

Models/References	Modelling dry soil	Absorption of water film	Irregular water film thickness	BRDF signatures
Ångström (Ångström, 1925)	×	√	×	×
Lekner & Dorf (1988)	×	√	×	×
Bach & Mauser (1994)	×	√	×	×
SPLITS (Kimmel & Baranoski, 2007)	√	√	√	√
Hapke (2012)	√	√	×	√
Sadeghi et al.(2017)	×	√	×	×
BSM (Verhoef et al., 2018)	√	√	√	×
MARMIT (Babliet et al., 2018)	×	√	√	×
Hapke-HSR (Ding et al., 2022)	√	√	×	√
MARMIT-2 (Dupiau et al., 2022)	×	√	√	×

64  
 65 The Hapke model has been widely applied in remote sensing for the retrieval of soil physical and biochemical  
 66 properties (Hapke, 2012; Zhao et al., 2023). Building on this framework, we previously developed a hyperspectral Hapke-  
 67 based formulation (the Hapke-HSR model) by establishing a wavelength-dependent representation of the single scattering  
 68 albedo (Ding et al., 2022), which enables improved simulation of dry soil spectral reflectance (SSR). Nevertheless, important  
 69 limitations remain in the representation of moisture-dependent soil reflectance. First, the Hapke-HSR model is primarily  
 70 parameterized for dry soil conditions, and its extension to wet soils relies on simplified assumptions. Second, the influence  
 71 of soil moisture is represented through an idealized surface water layer, which restricts the model’s ability to accurately  
 72 characterize reflectance variations across a broad range of SMC and leads to systematic biases in major water absorption  
 73 regions. Recently, the MARMIT-2 model has demonstrated strong performance in simulating SSR under varying moisture  
 74 conditions by incorporating reflectance properties from diverse soil types (Dupiau et al., 2022). However, the MARMIT-2  
 75 model does not explicitly represent angular effects and requires prior knowledge of dry soil reflectance, which is often  
 76 difficult to obtain from field or satellite observations. These limitations indicate that neither Hapke-HSR nor MARMIT-2



77 models alone provides a fully consistent framework for modeling soil reflectance under varying moisture conditions, thereby  
78 motivating the development of a unified soil modeling framework.

79 To address these issues, this study develops a unified modeling framework and formulates a physically coherent  
80 coupling strategy between the Hapke-HSR and MARMIT-2 models. We first refine the Hapke-HSR parameterization by  
81 exploiting the similarity between the spectral shapes of the single scattering albedo and dry soil reflectance. The improved  
82 Hapke-HSR model is then dynamically coupled with the MARMIT-2 model to enable joint simulation of soil spectral  
83 reflectance under both dry and wet conditions. This unified framework improves the physical consistency and numerical  
84 robustness of soil radiative transfer modeling and provides a reliable foundation for land surface parameter inversion in  
85 optical remote sensing.

## 86 2 Soil radiative transfer models

### 87 2.1 Hapke-HSR model

88 In the Hapke-HSR model, dry soil is treated as a semi-infinite horizontal surface containing irregularly and randomly  
89 distributed absorbing particles (Ding et al., 2022), and the formulas of this model are defined as follows:

$$R_d(\theta_s, \theta_v, \varphi, \lambda) = \frac{\omega}{4 \cos \theta_s + \cos \theta_v} \{ [P(g, g')(1 + B(g))] + H(\cos \theta_s)H(\cos \theta_v) - 1 \} \quad (1)$$

$$P(g, g') = 1 + b \cos g + \frac{c(3 \cos^2 g - 1)}{2} + b' \cos g' + \frac{c'(3 \cos^2 g' - 1)}{2} \quad (2)$$

$$\cos g = \cos \theta_s \cos \theta_v + \sin \theta_s \sin \theta_v \cos \varphi \quad (3)$$

$$\cos g' = \cos \theta_s \cos \theta_v - \sin \theta_s \sin \theta_v \cos \varphi \quad (4)$$

$$B(g) = \frac{B_0}{1 + \frac{1}{h} \tan\left(\frac{g}{2}\right)} \quad (5)$$

$$H(x) = \frac{1 + 2x}{1 + 2x\sqrt{1 - \omega}} \quad (6)$$

90 where  $R_d(\theta_s, \theta_v, \varphi, \lambda)$  represents dry soil reflectance,  $\omega$  represents the average SSA,  $B(g)$  is the hotspot function, and  $B_0 = 0.4$   
91 and  $h = 0.1$  are the optimal values.  $P(g, g')$  represents the scattering phase function, with optimal values assigned as follows:  
92  $b' = 0.4$ ,  $c = 0.4$ , and  $c' = 0$ . We employed the  $P(g, g')$  function in this study because it provides a more accurate  
93 representation of the anisotropic characteristics of soil.  $\theta_s$ ,  $\theta_v$ , and  $\varphi$  are the view zenith angle (VZA), solar zenith angle  
94 (SZA), and relative azimuth angle (RAA), respectively.

95 The relationship between the soil SSA and wavelength was established via radiative transfer theory. The association  
96 formulas of the SSA and wavelength are as follows:

$$\omega = 1 - \frac{4\pi M \chi_{soil}}{\lambda} \quad (7)$$

97 where  $M$  represents the soil particle size and shape-dependent parameter and  $\chi_{soil}$  is the soil refractive index, which is  
98 important for simulating soil optical properties.

99 In the Hapke-HSR model, the relationship between SSA ( $\omega$ ) and wavelength is further simplified as follows:

$$\omega_1 = 1 - \frac{1}{A_0 \lambda + A_1} \quad (8)$$



$$\omega_2 = 1 - \frac{1}{A_2\lambda + A_3} + \Delta d \quad (9)$$

100 where  $\Delta d$  refers to the offset of two soil spectra and where  $A_0, A_1, A_2$  and  $A_3$  represent the soil spectral parameters.

101 Considering the influence of SMC, we assume that the equivalent water thickness represents the transition from dry soil  
102 to wet soil (Yang et al., 2011). The formulas are defined as follows:

$$R_w(\theta_s, \theta_v, \varphi, \lambda) = R_d(\theta_s, \theta_v, \varphi, \lambda) \times e^{-\alpha_{\text{water}} f} \quad (10)$$

$$\alpha_{\text{water}} = \frac{4\pi\chi_{\text{water}}}{\lambda} \quad (11)$$

103 where  $R_w(\theta_s, \theta_v, \varphi, \lambda)$  represents wet soil reflectance,  $\chi_{\text{water}}$  is the water refractive index for water, and  $f$  is the equivalent  
104 water thickness.

## 105 2.2 Improvement of the Hapke-HSR model

106 The primary challenge in addressing the statistical relationship between the SSA and wavelength of the Hapke-HSR model is  
107 to provide a stable parameter  $\chi_{\text{soil}}$ . In this study, we assume that the shape of the dry SSR is consistent with the variation in  
108 the SSA with wavelength (Ding et al., 2022). A method is proposed to calculate the parameter  $\chi_{\text{soil}}$  via the dry SSR and  
109 improve the Hapke-HSR model. The SSA typically has a significant influence on the SSR, with multiple scattering events  
110 often disregarded in the theoretical derivation (Yang, 2022). The relationships between dry SSR and SSA are as follows:

$$R_d(\theta_s, \theta_v, \varphi, \lambda) = C_1 \times \omega \quad (12)$$

$$C_1 = \frac{1}{4(\cos\theta_s + \cos\theta_v)} \{ [P(g, g')(1 + B(g))] - 1 \} \quad (13)$$

$$\omega = 1 - \frac{C_2 \times \chi_{\text{soil}}}{\lambda} \quad (14)$$

$$C_2 = 4\pi M \quad (15)$$

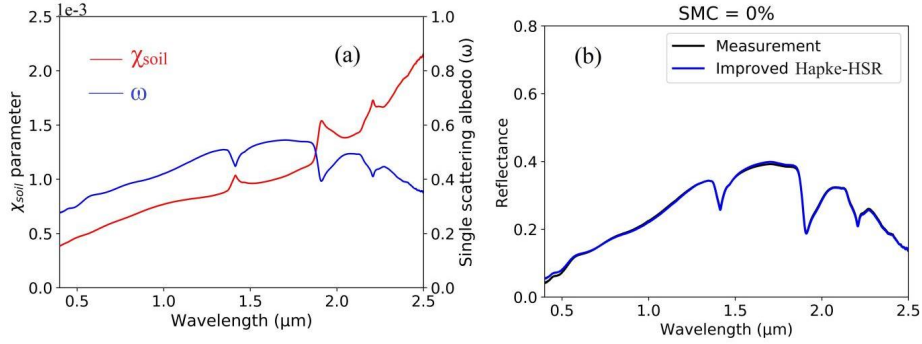
$$\chi_{\text{soil}} = \frac{\lambda}{C_2} \times \left( 1 - \frac{R_d(\theta_s, \theta_v, \varphi, \lambda)}{C_1} \right) \quad (16)$$

111 where  $C_1$  and  $C_2$  are the shape adjustment parameters of the dry SSR. We use  $C_1 = 1$  and  $C_2 = 1$  as the initial values to  
112 simplify the calculation, and we then further calculate the shape adjustment parameters.

113 To incorporate the impact of multiple scattering within the soil, we first calculate the  $\chi_{\text{soil}}$  parameter via Eq. (16). This  
114 parameter is then utilized in the improved Hapke-HSR model to determine the dry SSR. We adjust the dry SSR estimated  
115 with the improved Hapke-HSR model via the measured SSR and then calculate the adjusted dry SSR. The relationship  
116 between the dry SSR simulated via the improved Hapke-HSR model and the measured dry SSR can be expressed via the  
117 following formula:

$$R'_d(\theta_s, \theta_v, \varphi, \lambda) = C_3 \times R_d(\theta_s, \theta_v, \varphi, \lambda) + C_4 \quad (17)$$

118 where  $C_3$  and  $C_4$  represent the spectral shape adjustment parameters of the dry SSR. Note that  $R_d(\theta_s, \theta_v, \varphi, \lambda)$  is calculated  
119 via the improved Hapke-HSR model, and  $R'_d(\theta_s, \theta_v, \varphi, \lambda)$  represents the measured dry SSR.



120

121 **Figure 1: The variation in the soil refractive index (parameter  $\chi_{soil}$ ) and SSA of dry soil with wavelength (a). The**  
 122 **measured dry soil reflectance (i.e., dup20\_009) and soil reflectance calculated with the improved Hapke-HSR**  
 123 **model (b).**

124 Figure 1(a) shows the variation in the parameter  $\chi_{soil}$  and soil SSA calculated with the dry SSR (i.e., dup20\_009)  
 125 considering the wavelength. The parameter  $\chi_{soil}$  increases with wavelength, the slope clearly increases at wavelengths of 2.0–  
 126 2.5  $\mu\text{m}$ , and there are obvious peak values in the absorption band of water (centred at 1.47, 1.90 and 2.21  $\mu\text{m}$ ). The soil SSA  
 127 is highly similar to the dry SSR. With increasing wavelength, the SSA increases significantly in the spectral range of 0.4–  
 128 1.36  $\mu\text{m}$ . In the spectral range of 1.36–2.5  $\mu\text{m}$ , obvious valleys occur in the absorption band of water, which is similar to that  
 129 of dry SSR. In general, the SSA and dry SSR curves display very high similarity in terms of shape, but the SSA curve is  
 130 flatter. Figure 1(b) shows the measured dry SSR and the SSR estimated with the improved Hapke-HSR model. Clearly, the  
 131 SSR modelled by the improved Hapke-HSR model matches well with the measured dry SSR and can characterize the dry  
 132 SSR characteristics well. The accuracy of this improved model in fitting these typical data is shown in Table 4 ( $R^2 = 1.00$ ,  
 133 RMSE = 0.001). These analyses suggest that calculating the parameter  $\chi_{soil}$  via dry SSR data is feasible and can solve the  
 134 problems associated with the statistical relationship between the SSA and wavelength of the Hapke-HSR model.

### 135 2.3 Coupling strategy between the improved Hapke-HSR and MARMIT-2 models

#### 136 (1) Physical coupling mechanism between the improved Hapke-HSR model and MARMIT-2 model

137 The improved Hapke-HSR model provides an effective description of multi-angular dry soil spectral reflectance, whereas the  
 138 MARMIT-2 model explicitly accounts for the influence of SMC on soil reflectance but assumes that dry reflectance is  
 139 known and does not incorporate directional information. By coupling these two models, their complementary strengths can  
 140 be integrated to achieve a more physically consistent representation of both the spectral and moisture-dependent behavior of  
 141 soils. In the proposed framework, dry soil reflectance under different viewing geometries is first simulated using the  
 142 improved Hapke-HSR model and subsequently used as input to the MARMIT-2 model. As a result, the MARMIT-2 model  
 143 no longer requires externally prescribed dry reflectance. Moreover, because the simulations of the Hapke-HSR model retain  
 144 angular information, the coupled Hapke-HSR + MARMIT-2 model is able to account for the influence of observation  
 145 geometry on soil reflectance. Through this coupling strategy, the reflectance properties of both dry and wet soils can be  
 146 simulated under varying angular and moisture conditions within a unified framework (Ding, 2025).

#### 147 (2) Radiative transfer formulation of the coupled Hapke-HSR + MARMIT-2 model

148 In the MARMIT-2 model, wet soil is described as dry soil overlaid with a thin layer of water (Dupiau et al., 2022). Therefore,  
 149 the wet SSR is described as follows:

$$R_{mod}(\theta_s, \theta_v, \varphi, \lambda) = \varepsilon R_w(\theta_s, \theta_v, \varphi, \lambda) + (1 - \varepsilon) R_d(\theta_s, \theta_v, \varphi, \lambda) \quad (18)$$

150 where  $R_m(\theta_s, \theta_v, \varphi, \lambda)$  is the wet SSR,  $R_d(\theta_s, \theta_v, \varphi, \lambda)$  is the dry SSR calculated via the improved Hapke-HSR model,  $R_w(\theta_s,$   
 151  $\theta_v, \varphi, \lambda)$  refers to the fully wet SSR,  $\varepsilon$  is the wet soil fraction, and  $R_w(\theta_s, \theta_v, \varphi, \lambda)$  is described as:



$$R_w(\theta_s, \theta_v, \varphi, \lambda) = \frac{t_{12}t_{21}R_d(\theta_s, \theta_v, \varphi, \lambda)T_w^2}{1 - r_{21}R_d(\theta_s, \theta_v, \varphi, \lambda)T_w^2} \quad (19)$$

152 where  $t_{12}$  and  $t_{21}$  are the interface transmittance of light passing into and out of the water layer, respectively.

153 To address the presence of multiple scattering events within the water layer, transmittance ( $T_w$ ) is considered.

$$T_w = (1 - \alpha_{water}L)e^{-\alpha_{water}L} + \alpha_{water}L \int_{\alpha_{water}L}^{\infty} \frac{e^{-x}}{x} dx \quad (20)$$

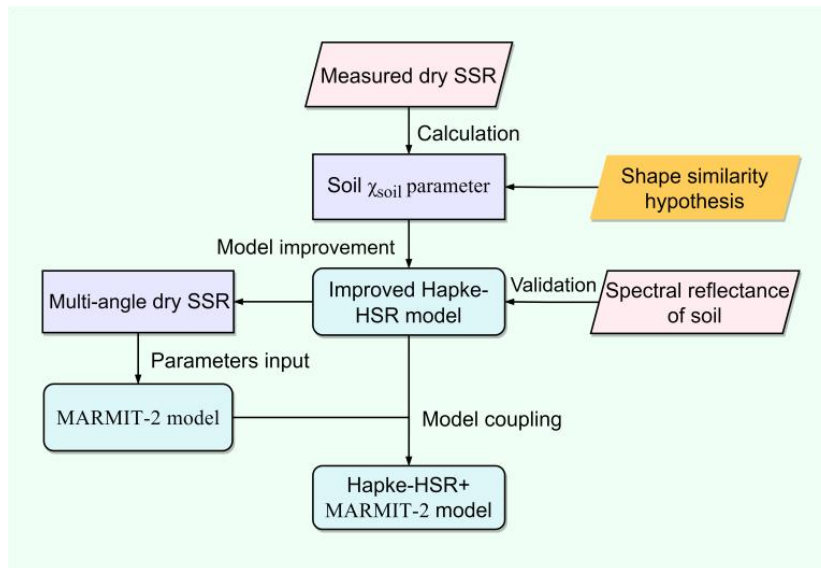
154 where  $L$  refers to the water layer thickness.

$$n_{mix} = \delta n_{soil} + (1 - \delta)n_{water} \quad (21)$$

155 where  $n_{mix}$  represents the result of the linear weighting of the complex refractive index of water and soil,  $n_{soil}$  and  $n_{water}$   
 156 represents the complex refractive index of water and soil particles respectively, and  $\delta$  represents the volume fraction of soil  
 157 particles.

### 158 (3) Computational procedure and evaluation scheme

159 Figure 2 illustrates the workflow of the improved Hapke-HSR model and its coupling with the MARMIT-2 model. First, the  
 160 soil parameter  $\chi_{soil}$  is estimated from measured dry SSR by assuming similarity between the spectral shapes of the single-  
 161 scattering albedo and dry SSR. The derived  $\chi_{soil}$  is then incorporated into the Hapke-HSR model, which alleviates the  
 162 limitations associated with piecewise fitting of the single scattering albedo and improves the numerical stability of the  
 163 formulation. The refined Hapke-HSR model is subsequently used to simulate dry SSR under different viewing geometries,  
 164 and these simulations are provided as input to the MARMIT-2 model, thereby enabling the dynamic coupling of the two  
 165 formulations. Finally, the performance of the coupled Hapke-HSR + MARMIT-2 model is evaluated using eight independent  
 166 soil spectral databases spanning a range of soil moisture conditions. Model performance is assessed using multiple statistical  
 167 metrics, including the coefficient of determination ( $R^2$ ), root mean square error (RMSE), normalized RMSE (NRMSE),  
 168 mean relative error (MRE), and bias.



169

170 **Figure 2: The workflow of the improved Hapke-HSR model and the coupled MARMIT-2 model.**



171 **3 Databases and methods**

172 **3.1 Databases of soil spectral reflectance**

173 In this section, eight different databases provided by Dupiau et al. (2022) are used to verify the Hapke-HSR + MARMIT-2  
 174 model (Table 2). These eight datasets were acquired primarily via the Analytical Spectra Devices (ASD) FieldSpec  
 175 spectroradiometer. The soil types in the datasets are diverse, consisting primarily of clay, silt, and sand as the main  
 176 components. The Bab16, Dup20, and Liu02 databases provide the soil components of each sample, such as organic matter,  
 177 iron, nitrogen and organic carbon. These eight databases provide dry and wet SSR data for 219 soil samples, spanning 1984  
 178 spectra in the 0.4-2.5  $\mu\text{m}$  range. The data quality of these databases is high, but there are some uncertainties in the 2.4-2.5  
 179  $\mu\text{m}$  range. Therefore, these databases offer crucial data for validating the ability of the Hapke-HSR + MARMIT-2 model to  
 180 describe SSR features.

181 **Table 2.** The main information on the eight soil databases.

Databases	Locations	Number of soil spectrum	Spectral range ( $\mu\text{m}$ )	Spectral resolution ( $\mu\text{m}$ )	SMCg (%)
Bab16	ONERA, Toulouse (France)	106	0.4-2.4	0.001	0-79.2
Dup20	ONERA, Toulouse (France)	72	0.4-2.5	0.001	0-68.91
Hum15	ONERA, Toulouse (France)	455	0.4-2.298	0.001	0-67
Les08	ONERA, Toulouse (France)	190	0.4-2.4	0.001	0-87
Liu02	INRAE, Avignon (France)	367	0.4-2.4	0.001	0-81.1
Lob02	Standford University, Standford (CA, USA)	41	0.4-2.49	0.001	0-109.4
Mar12	CEA, Bruyères le Chatel (France)	258	0.4-2.4	0.001	0-52.9
Phil14	Cornell University, Ithaca (NY, USA)	405	0.4-2.5	0.001	0-50.71

182 Note: SMCg is the soil moisture content (SMC) as a weight percent.

183 **4 Results and analysis**

184 **4.1 Parameters analysis of the Hapke-HSR + MARMIT-2 model**

185 In this section, we first analyse the effects of the main input parameters of the Hapke-HSR + MARMIT-2 (HM) model on  
 186 the soil reflectance properties. Table 3 shows the main input variables of the HM model. The Hapke-HSR model has many  
 187 input variables, and the variables of this model were optimized in previous studies (Ding et al., 2022); five main variables  
 188 were used to describe the soil spectral and angular features. The MARMIT-2 model includes three main parameters that  
 189 describe the influence of the SMC on SSR. We analyse the effects of different parameters in the HM model on the simulated  
 190 SSR.

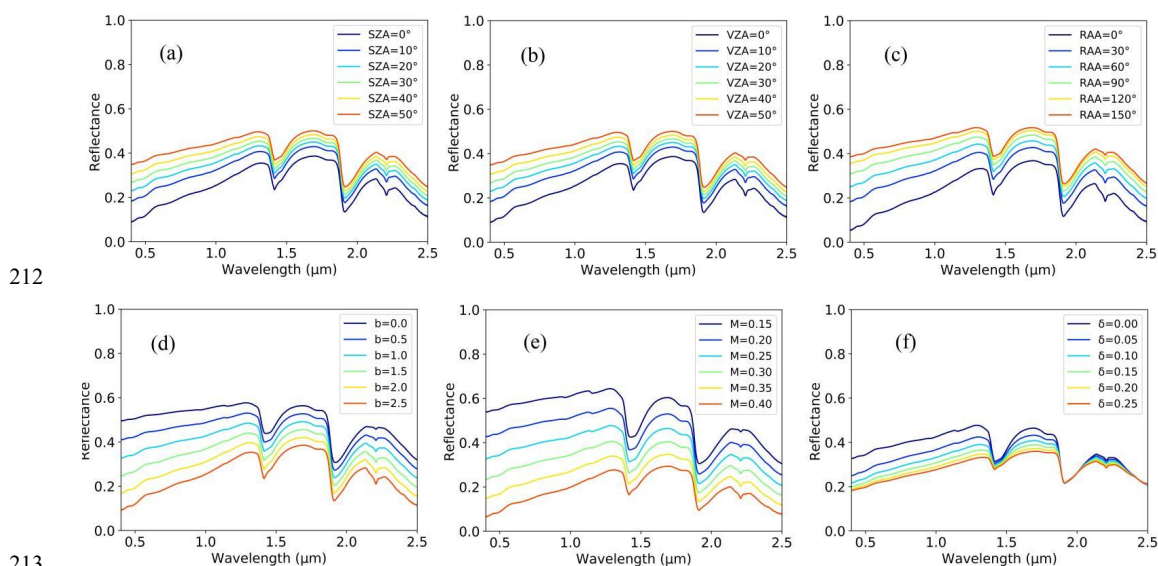
191 **Table 3.** The main input variables of the Hapke-HSR + MARMIT-2 (HM) model.

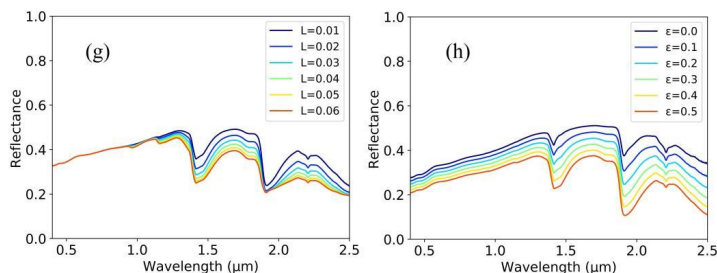
Databases	Parameters	Range of values	Units
Hapke-HSR	Solar zenith angle (SZA)	0-90	degrees ( $^{\circ}$ )
	View zenith angle (VZA)	0-90	degrees ( $^{\circ}$ )
	Relative azimuth angle (RAA)	0-180	degrees ( $^{\circ}$ )
	The coefficient of the scattering phase function ( $b$ )	0-6	--
	Soil particle size and shape-dependent parameter ( $M$ )	0-1	mm



	Volume fraction of soil particles ( $\delta$ )	0-0.25	--
MARMIT-2	Thickness of water layer ( $L$ )	0-0.15	cm
	Surface coverage fraction of water ( $\epsilon$ )	0-1	--

192 Figure 3 illustrates the impact of the main variables of the Hapke-HSR + MARMIT-2 (HM) model on the SSR. For the  
 193 influence of angle variation, the SSR calculated via the HM model increases with increasing SZA parameters. The increase  
 194 in SSR is obvious in the range of 0.4–1.36  $\mu\text{m}$ ; however, the rate of increase in SSR subsequently decreases. The impact of  
 195 VZA parameters on SSR is consistent with the influence of the SZA parameters since the Hapke-HSR model is reciprocal.  
 196 Furthermore, the influence of the RAA parameters on SSR is basically the same as that of the SZA parameters with  
 197 increasing RAA parameters; however, the changes in soil reflectance are slightly different. With increasing parameter  $b$ , the  
 198 SSR determined via the HM model decreases, and the decrease in SSR is obvious in the range of 0.4–1.36  $\mu\text{m}$ , whereas the  
 199 decrease in SSR is weak in the range of 1.36–2.5  $\mu\text{m}$ . The SSR simulated with the HM model also decreases with increasing  
 200  $M$ ; this finding corroborates the experimental observations regarding spectral variations due to soil particle size reported by  
 201 Sun et al.(2023). However, the variation in the parameter  $M$  of the SSR is basically the same at different wavelengths. A  
 202 possible reason is that the influence of the parameter  $M$  in the range of 0.4-2.5  $\mu\text{m}$  on the SSR is consistent, which may be  
 203 related to the structure of Eq. (7). For the variables related to the SMC, with increasing parameter  $\delta$ , the SSR decreases,  
 204 whereas in the strong absorption band of water, this effect is smaller. A possible reason for this result is that the absorption  
 205 of water weakens the impact of the parameter  $\delta$  on the SSR. As the parameter  $L$  increases, the SSR decreases in the range of  
 206 1.0–2.5  $\mu\text{m}$ , whereas the variation in the parameter  $L$  has no effect on the soil reflectance in the range of 0.4–1.0  $\mu\text{m}$ . With  
 207 increasing parameter  $\epsilon$ , the SSR decreases. In the strong absorption band of water, the simulated SSR quickly decreases. In  
 208 summary, the main parameters of the Hapke-HSR model are related to the influence of dry SSR and angular variation  
 209 characteristics, and the variables of the MARMIT-2 model mainly account for the influence of SMC on the SSR. Therefore,  
 210 the HM model can characterize the spectral and angular reflectance attributes of dry and wet soils by coupling the Hapke-  
 211 HSR and MARMIT-2 models.





214

215 **Figure 3: Influence of the SZA (a), VZA (b), RAA (c),  $b$  (d),  $M$  (e),  $\delta$  (f), and  $\varepsilon$  (h) in the Hapke-HSR + MARMIT-2**  
 216 **(HM) model on soil reflectance.**

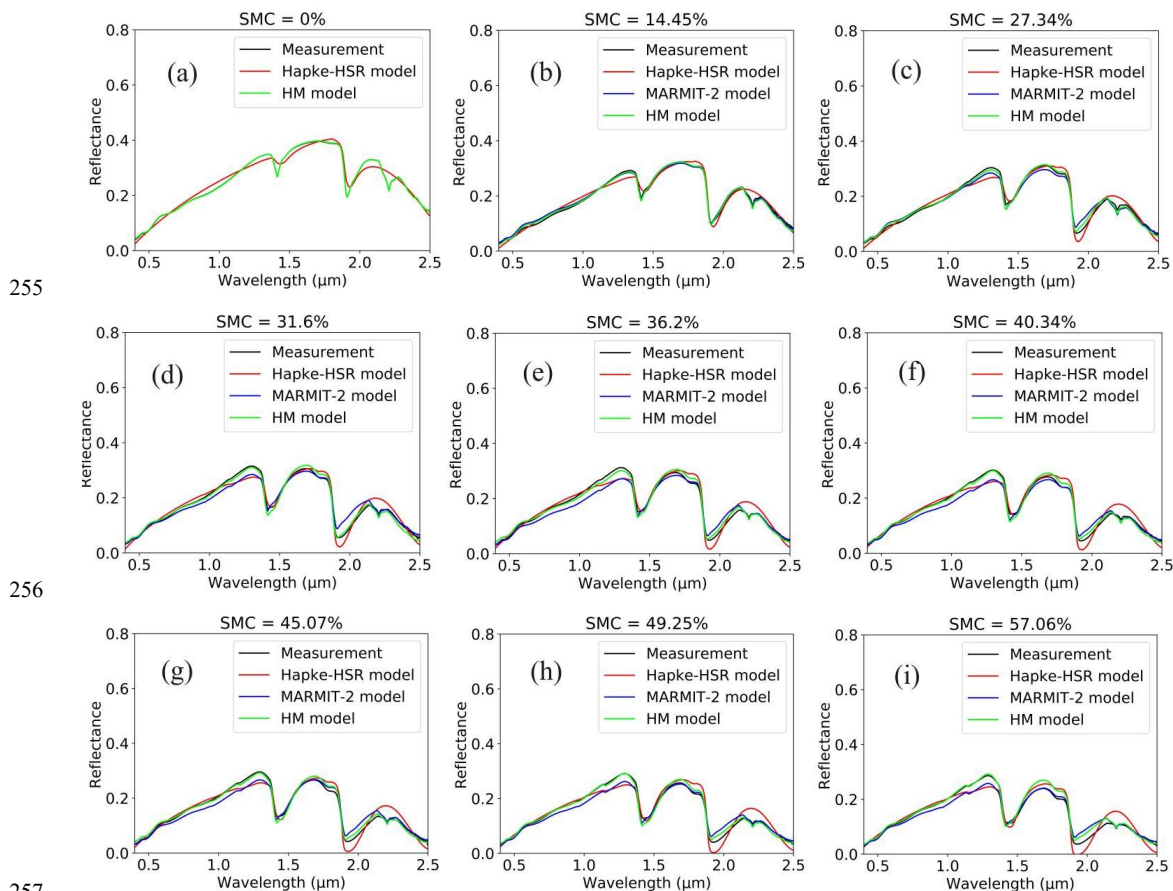
217 **4.2 Validating the Hapke-HSR + MARMIT-2 model to describe soil reflectance properties**

218 In previous studies, we assessed the Hapke-HSR model to describe soil BRDF features (Ding et al., 2022). Therefore, we  
 219 focus mainly on evaluating the soil spectral characteristics in this paper. In addition, these eight soil databases do not provide  
 220 angle-related information. Therefore, we use  $SZA = 45^\circ$ ,  $VZA = 0^\circ$  and  $RAA = 0^\circ$  as fixed values because SSR is usually  
 221 measured in the nadir direction. Figure 4 shows that the Hapke-HSR, MARMIT-2 and Hapke-HSR + MARMIT-2 (HM)  
 222 models effectively fit the influence of the typical fitted SSR (dup20\_009-001) at SMCs = 0%, 14.45%, 27.34%, 31.6%,  
 223 36.2%, 40.34%, 45.07%, 49.25%, and 57.06%, respectively. The SSR decreases significantly with increasing SMC, and the  
 224 main absorption bands (centred at 1.47 and 1.90  $\mu\text{m}$ ) of water become wider. The outcomes simulated using the Hapke-HSR,  
 225 MARMIT-2 and HM models can be used to determine the change in SSR with increasing SMC and are highly in line with  
 226 the measured SSR values. On the basis of a comparison of the results, the HM model fits the measured SSR better than the  
 227 Hapke-HSR and MARMIT-2 models do, especially at  $SMC \geq 30\%$ . Compared with the MARMIT-2 model, the HM model  
 228 yields slightly better results. The main reason is that the MARMIT-2 model yields very high accuracy in characterizing SSR  
 229 characteristics. The ability of the Hapke-HSR model to accurately fit the measured SSR decreases with increasing SMC. The  
 230 correlation analysis results indicate that the fitting ability of these two models meets the relevant requirements. However, at  
 231  $SMC \geq 30\%$ , the fitting capability of the MARMIT-2 model is relatively low due to slight underestimations in the range of  
 232 0.4-1.36  $\mu\text{m}$ , and there is an overestimation in the strong water absorption band; moreover, the Hapke-HSR model has  
 233 difficulty capturing the SSR characteristics in the absorption band of water, which leads to significant underestimation of the  
 234 fitted SSR at a wavelength of approximately 1.90  $\mu\text{m}$ . However, the HM model effectively considers the influence of these  
 235 factors, resulting in high accuracy for characterizing SSR attributes. To show the differences between the SSR values  
 236 simulated with these three models and the measured spectral reflectance values, we calculate the bias between them, as  
 237 shown in Appendix Figure A1. In addition, the Hapke-HSR and HM models are applied to simulate the dry SSR, and the  
 238 SSR simulated via the HM model is more consistent with the measured results than the SSR obtained with the Hapke-HSR  
 239 model is.

240 Table 4 shows that the Hapke-HSR, MARMIT-2 and HM models fit the parameters and statistical results of the SSR.  
 241 With increasing SMC, the parameters  $L$  and  $\varepsilon$  in the MARMIT-2 model increase significantly, whereas the parameter  $\delta$   
 242 shows little variation. The parameter  $f$  increases significantly. Moreover, the SSR fitting accuracy of the Hapke-HSR and  
 243 MARMIT-2 models decreases with increasing SMC, especially at  $SMC \geq 30\%$ . This finding may be because the MARMIT-  
 244 2 model ignores the variations in soil scattering characteristics, particle size and shape with increasing SMC. In the Hapke-  
 245 HSR model, a dry soil surface is overlaid with a water layer to reflect the influence of the SMC on the SSR. This simple  
 246 assumption limits the ability of the Hapke-HSR model to fit the variable characteristics of the SMC. The overall  $R^2$  values  
 247 for the Hapke-HSR model in SSR fitting vary from 0.952 to 0.971, with RMSE values varying from 0.016 to 0.019, and the  
 248 MARMIT-2 model achieves  $R^2$  values between 0.957 and 0.995 in SSR fitting, with RMSE values ranging from 0.007 to



249 0.021 and negligible bias. These results indicate that these two models can effectively characterize the variation in SSR with  
 250 SMC and yield high fitting accuracy. However, the HM model is accurate (RMSE = 0.008), presenting a high  $R^2$  ( $R^2 = 0.991$ )  
 251 and a small bias in relation to the measured SSR. This is because the HM model considers the variations in the soil scattering  
 252 characteristics, particle size and particle shape with increasing SMC. Therefore, the HM model can effectively characterize  
 253 the attributes of SSR and exhibits greater accuracy than the Hapke-HSR and MARMIT-2 models do, especially at  $SMC \geq$   
 254 30%.



257  
 258 **Figure 4:** The Hapke-HSR (red), MARMIT-2 (blue) and Hapke-HSR + MARMIT-2 (HM) (lime) models fit the  
 259 measured soil reflectance (black) at SMC = 0% (a), 14.45% (b), 27.34% (c), 31.6% (d), 36.2% (e), 40.34% (f), 45.07%  
 260 (g), 49.25% (h), and 57.06% (i), respectively.

261 **Table 4.** The Hapke-HSR, MARMIT-2 and Hapke-HSR + MARMIT-2 (HM) models fit the soil reflectance variables and  
 262 statistical outcomes.

Models	SMC (%)	$b$	$f/M$	$A_0/\delta$	$A_1/L$	$A_2/\epsilon$	$A_3$	$R^2$	RMSE	bias
Hapke-HSR	0.0	4.4	0.4	0.782	0.723	-1.141	4.178	0.972	0.016	0.001
	14.45	4.8	1.0	0.545	0.796	-0.708	3.054	0.976	0.013	0.001
	27.34	3.0	1.6	0.861	0.677	-1.151	4.336	0.968	0.016	0.000
	31.6	1.4	2.0	1.586	0.405	-1.908	6.738	0.962	0.019	0.001
	36.2	1.6	2.2	1.431	0.479	-1.795	6.326	0.954	0.020	0.002
	40.34	1.0	2.4	1.699	0.392	-1.924	6.948	0.948	0.020	0.002

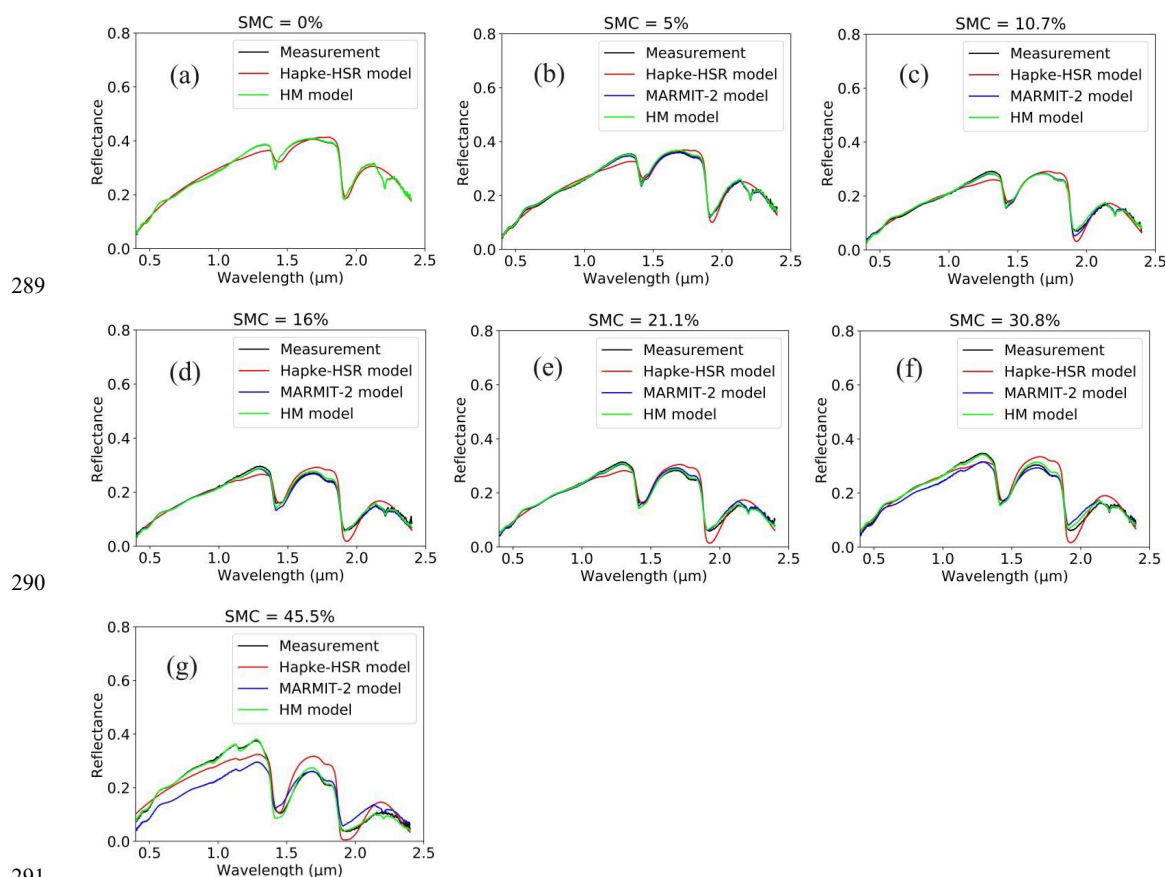


	45.07	0.0	2.8	2.772	-0.009	-2.420	9.426	0.945	0.021	0.001
	49.25	0.8	2.8	1.747	0.384	-1.757	6.801	0.938	0.022	0.001
	57.06	0.2	3.4	2.316	0.188	-1.390	7.026	0.936	0.023	0.001
	All	--	--	--	--	--	--	0.952	0.019	0.001
	0	--	--	--	--	--	--	--	--	--
	14.45	--	--	0.030	0.01	0.3	--	0.995	0.007	0.001
	27.34	--	--	0.000	0.03	0.3	--	0.984	0.013	-0.002
	31.6	--	--	0.000	0.03	0.3	--	0.957	0.019	-0.002
	36.2	--	--	0.000	0.02	0.4	--	0.955	0.021	-0.008
MARMIT-2	40.34	--	--	0.000	0.03	0.4	--	0.970	0.018	-0.008
	45.07	--	--	0.000	0.03	0.4	--	0.956	0.018	-0.003
	49.25	--	--	0.000	0.04	0.4	--	0.969	0.017	-0.005
	57.06	--	--	0.000	0.05	0.4	--	0.957	0.018	-0.002
	All	--	--	--	--	--	--	0.971	0.016	-0.003
	0	2.0	0.30	0.000	0.00	0.0	--	1.000	0.001	0.000
	14.45	2.2	0.29	0.018	0.01	0.3	--	0.994	0.006	-0.001
	27.34	3.1	0.24	0.011	0.02	0.4	--	0.991	0.008	0.000
	31.6	4.0	0.21	0.006	0.02	0.5	--	0.989	0.009	-0.001
Hapke-HSR + MARMIT- 2	36.2	3.3	0.23	0.000	0.02	0.5	--	0.986	0.010	0.000
	40.34	4.0	0.21	0.006	0.03	0.5	--	0.987	0.009	0.000
	45.07	3.3	0.23	0.001	0.03	0.5	--	0.987	0.009	0.002
	49.25	4.0	0.21	0.005	0.04	0.5	--	0.986	0.009	0.001
	57.06	3.7	0.22	0.000	0.05	0.5	--	0.984	0.009	-0.001
	All	--	--	--	--	--	--	0.991	0.008	0.000

263 Figure 5 shows that the Hapke-HSR, MARMIT-2 and HM models fit the typical measured SSR (bab16\_014-008) at  
 264 SMC = 0%, 5%, 10.7%, 16%, 21.1%, 30.8%, and 45.5%, respectively. This set of typical data is suspected to have a specular  
 265 reflection effect when SMC = 30.8% and 45.5%. Therefore, we further validate the capacity of the HM model for describing  
 266 the relevant SSR attributes. The outcomes of the Hapke-HSR, MARMIT-2 and HM models match the typical measured SSR  
 267 when the SMC < 30%. The Hapke-HSR and MARMIT-2 models cannot effectively consider the specular reflectance  
 268 characteristics at high SMCs, and the results of the HM model display greater consistency with the measured SSR values.  
 269 When the SMC is high and there is a specular reflectance effect, the fitting capability of the Hapke-HSR model is  
 270 significantly underestimated in the range of 0.5-1.2  $\mu\text{m}$  and two strong water absorption bands; moreover, there is a slight  
 271 overestimation in the range of 1.5-1.9  $\mu\text{m}$ . The outcomes of the MARMIT-2 model are marginally underestimated across the  
 272 0.4-1.36  $\mu\text{m}$  interval, and there is a slight overestimation across the spectral interval of 1.36-2.5  $\mu\text{m}$ , particularly in the  
 273 strong water absorption region. The HM model can match the measured SSR well, especially at SMC = 30.8% and 45.5%,  
 274 possibly because this model accounts for the specular scattering characteristics of high SMCs on the basis of the coefficient  
 275 (b) and soil particle shape-dependent parameter (*M*). To better show the differences between the SSR values simulated with  
 276 these three models and the measured SSR values, we calculate the bias between them, as shown in Appendix Figure A2. The  
 277 results indicate that the HM model can describe SSR features effectively at SMC  $\geq$  30%, and the simulated values exhibit  
 278 very high consistency with the measured SSR values.



279 Table 5 shows that the Hapke-HSR, MARMIT-2 and HM models fit to the SSR parameters and statistical results. The  
 280 overall precision of the Hapke-HSR and MARMIT-2 models in terms of fitting measured SSR was high ( $R^2 = 0.943-0.946$ ,  
 281  $RMSE = 0.006-0.022$ ), especially at  $SMC < 30\%$ ; however, these two models were not suitable at  $SMC \geq 30\%$ , which needs  
 282 to be improved by accounting for specular reflectance. The HM model shows greater accuracy in fitting the variation in the  
 283 SMC than the Hapke-HSR and MARMIT-2 models; the overall  $R^2$  is 0.995, the RMSE is 0.009, and the bias is negligible.  
 284 When  $SMC = 30.8\%$  and  $45.5\%$ , the measured SSR are suspected to have a specular reflection effect, and the HM model  
 285 maintains a higher fitting precision ( $R^2 = 0.990-0.993$ ,  $RMSE = 0.009$ ) than the Hapke-HSR and MARMIT-2 models ( $R^2 =$   
 286  $0.846-0.973$ ,  $RMSE = 0.019-0.053$ ). These results indicate that these two models can be combined by coupling the Hapke-  
 287 HSR and MARMIT-2 models (i.e., HM model), which can effectively determine the variation in SSR with increasing SMC,  
 288 particularly in the presence of specular reflectance.



291  
 292 **Figure 5:** The Hapke-HSR (red), MARMIT-2 (blue) and Hapke-HSR + MARMIT-2 (HM) (lime) models fit the  
 293 measured soil reflectance (black) at  $SMC = 0\%$  (a),  $5\%$  (b),  $10.7\%$  (c),  $16\%$  (d),  $21.1\%$  (e),  $30.8\%$  (f), and  $45.5\%$  (g),  
 294 respectively.

295 **Table 5.** The Hapke-HSR, MARMIT-2 and Hapke-HSR + MARMIT-2 (HM) models fit to the soil reflectance parameters  
 296 and statistical results.

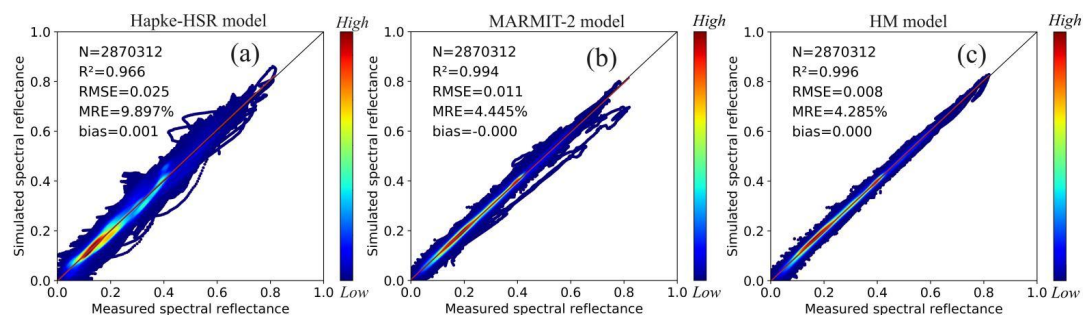
Models	SMC (%)	$b$	$f/M$	$A_0/\delta$	$A_1/L$	$A_2/\epsilon$	$A_3$	$R^2$	RMSE	bias
Hapke- HSR	0.0	1.4	0.6	2.447	0.180	-4.150	12.010	0.974	0.014	0.000
	5.0	1.4	1.0	2.016	0.322	-3.477	10.222	0.971	0.014	-0.001



	10.7	0.0	1.6	2.685	0.091	-5.119	14.339	0.960	0.015	-0.002
	16.0	0.2	2.0	2.506	0.189	-4.601	13.129	0.944	0.018	0.001
	21.1	0.0	2.2	3.144	-0.023	-5.618	15.939	0.941	0.020	0.000
	30.8	0.2	2.4	3.544	-0.173	-6.051	17.081	0.936	0.023	0.003
	45.5	1.0	4.0	2.377	0.439	-4.292	12.350	0.884	0.037	0.004
	All	--	--	--	--	--	--	0.943	0.022	0.001
	0.0	--	--	--	--	--	--	--	--	--
	5.0	--	--	0.000	0.01	0.2	--	0.996	0.006	-0.001
	10.7	--	--	0.020	0.01	0.5	--	0.993	0.006	-0.001
MARMIT-	16.0	--	--	0.010	0.03	0.4	--	0.991	0.009	-0.005
2	21.1	--	--	0.000	0.02	0.4	--	0.988	0.009	0.002
	30.8	--	--	0.000	0.04	0.3	--	0.973	0.019	-0.009
	45.5	--	--	0.000	0.04	0.4	--	0.846	0.053	-0.024
	All	--	--	--	--	--	--	0.946	0.022	-0.005
	0.0	2.0	0.30	0.000	0.00	0.0	--	1.000	0.001	0.000
	5.0	2.3	0.28	0.020	0.01	0.2	--	0.997	0.005	0.002
Hapke-	10.7	1.3	0.38	0.001	0.02	0.3	--	0.994	0.006	0.000
HSR +	16.0	1.7	0.33	0.000	0.02	0.4	--	0.991	0.007	-0.001
MARMIT-	21.1	2.4	0.27	0.009	0.03	0.4	--	0.992	0.007	0.000
2	30.8	3.0	0.24	0.002	0.03	0.4	--	0.990	0.009	0.002
	45.5	5.8	0.17	0.002	0.05	0.6	--	0.993	0.009	-0.002
	All	--	--	--	--	--	--	0.995	0.007	0.000

297

298 Figure 6 presents a comparison of the SSR results obtained from the Hapke-HSR, MARMIT-2 and HM models and the  
 299 measured SSR values from eight databases. These three models are generally highly accurate in terms of capturing SSR  
 300 features. However, the HM and MARMIT-2 models ( $R^2 = \sim 0.993$ ) fit the measured SSR data with slightly greater  
 301 correlation accuracy than did the Hapke-HSR model ( $R^2 = 0.957$ ), and the RMSE values of the HM (RMSE = 0.010) and  
 302 MARMIT-2 (RMSE = 0.012) models were significantly lower than the RMSE of the Hapke-HSR (RMSE = 0.027) model.  
 303 Additionally, the MRE values of the HM and MARMIT-2 models are approximately 5.74% and 6.43% lower than that of the  
 304 Hapke-HSR model, respectively. These findings indicate that the HM model yields the highest level of accuracy in fitting the  
 305 measured SSR, followed by the MARMIT-2 model, whereas the Hapke-HSR model has the worst fitting effect on the basis  
 306 of the measured SSR. The main reason is that the Hapke-HSR model includes a simple assumption regarding the effect of  
 307 the SMC on SSR. In addition, the SSR simulated by the Hapke-HSR and MARMIT-2 models is considerably uncertain at  
 308 high SMCs (e.g., Figure 5(f)-(g)), whereas the HM model results display greater consistency with the fitted SSR value. In  
 309 general, the HM and MARMIT-2 models excellently characterize the SSR attributes of soil and yield greater accuracy than  
 310 the Hapke-HSR model for the eight soil databases does, and the SSR estimates produced by the HM model are marginally  
 311 more accurate than those of the MARMIT-2 model are.

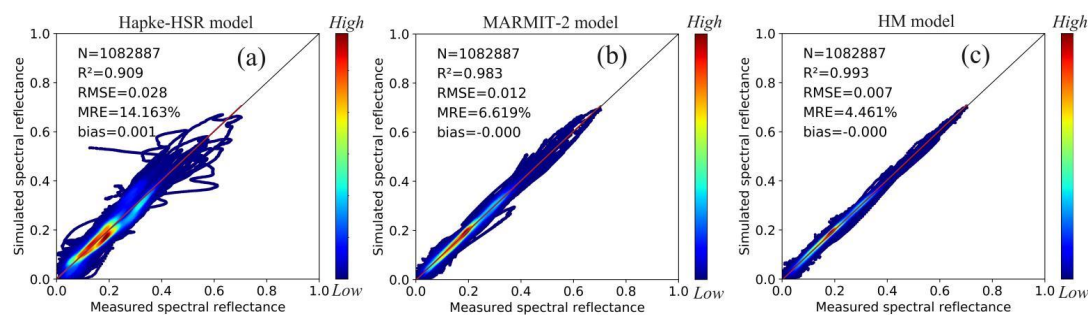


312

313 **Figure 6: Comparison results of the all soil reflectance simulated by the Hapke-HSR (a), MARMIT-2 (b) and Hapke-**  
 314 **HSR + MARMIT-2 (HM) (c) models with all measured soil reflectance.**

315 **4.3 Validating the Hapke-HSR + MARMIT-2 model for high SMC**

316 The MARMIT-2 and HM models achieve excellent fitting accuracy at SMC levels ranging from 030%, whereas the Hapke-  
 317 HSR and MARMIT-2 models exhibit moderate fitting capability at SMC ≥ 30% (e.g., Figures 3 and 4). Therefore, focus is  
 318 placed on comparing the fitting results of the above three models under the condition of an SMC ≥ 30%. Figure 7 shows the  
 319 comprehensive results obtained with the Hapke-HSR, MARMIT-2 and HM models at SMC ≥ 30%, and these three models  
 320 exhibit strong agreement with the measured SSR (R<sup>2</sup> > 0.90), with RMSE values ranging from 0.0070.028. However, the  
 321 accuracy of the HM model (R<sup>2</sup> = 0.993, RMSE = 0.007) for fitting SSR data is slightly better than that of the MARMIT-2  
 322 model (R<sup>2</sup> = 0.983, RMSE = 0.012) and significantly greater than that of the Hapke-HSR model (R<sup>2</sup> = 0.909, RMSE = 0.028).  
 323 Compared with those of the MARMIT-2 and Hapke-HSR models, the RMSE values of the HM model are 41.7% and 66.7%  
 324 lower, and the MRE values are 2.158% and 9.702% lower, respectively. Moreover, the HM model has the ability to  
 325 improved the inadequate fitting outcomes of the Hapke-HSR model. These findings show that the HM model can describe  
 326 SSR attributes more effectively than the other models can, especially at SMC ≥ 30%. The key factor is that the HM model  
 327 combines the strengths of both the Hapke-HSR and MARMIT-2 models to better describe the changes in SSR with  
 328 increasing SMC. The MARMIT-2 model also exhibits higher accuracy at SMC ≥ 30% since it fully considers the effect of  
 329 the SMC on SSR.



330

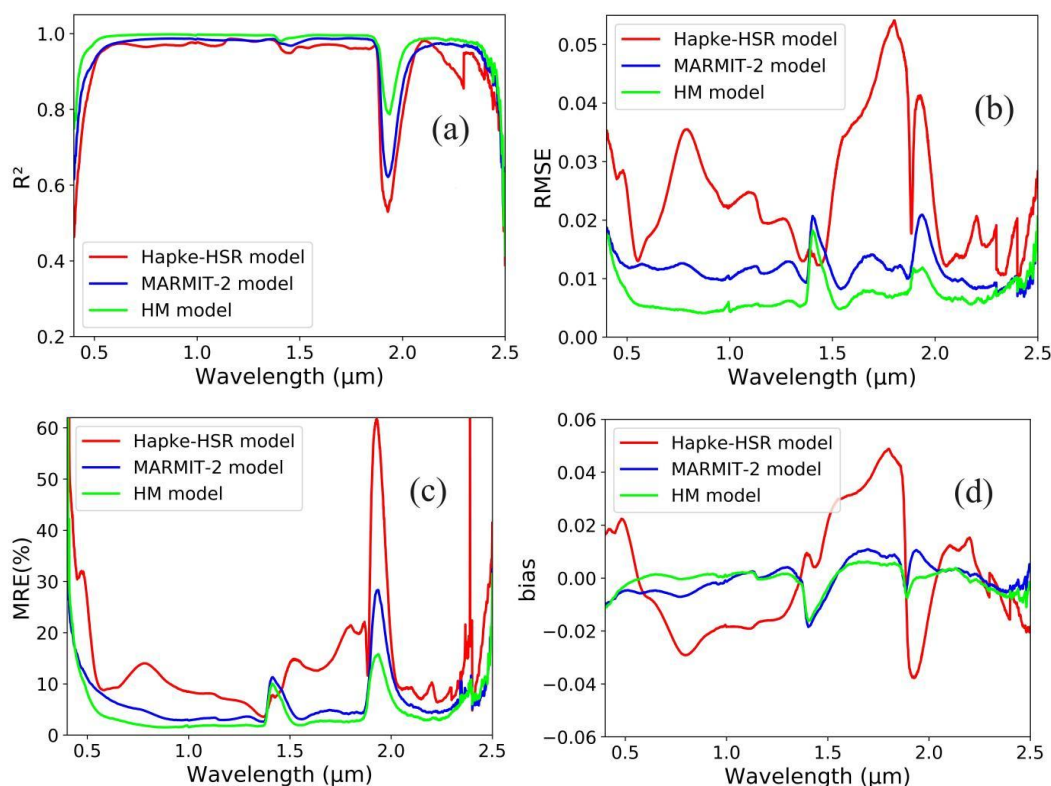
331 **Figure 7: Comparison results of the soil reflectance values simulated by the Hapke-HSR (a), MARMIT-2 (b) and**  
 332 **Hapke-HSR + MARMIT-2 (HM) (c) models with the measured soil reflectance at SMC ≥ 30%.**

333 Next, we further evaluate the ability of the Hapke-HSR, MARMIT-2 and HM models to fit the measured SSR for  
 334 different bands (0.4-2.5 μm) at SMC ≥ 30%. Figure 8 shows the comparison results between the simulated SSR values of the  
 335 three models and the measured SSR values. The results of these three models are highly consistent with the measured values.  
 336 The R<sup>2</sup> values of these three models are generally very high, in the range of 0.4–2.5 μm. The R<sup>2</sup> value of the HM model is  
 337 the largest, followed by those of the MARMIT-2 model and, finally, the Hapke-HSR model. However, the consistency



338 between the outcomes of these three models and the measured values in the strong absorption band of water (centred at 1.90  
339  $\mu\text{m}$ ) is significantly lower than that for the other bands. The RMSE results from the HM model were the smallest, followed  
340 by those of the MARMIT-2 model. The maximum RMSE value of the Hapke-HSR model was approximately 0.05 because  
341 the Hapke-HSR model uses a simplistic assumption to reflect the effect of the SMC. However, the HM and MARMIT-2  
342 models significantly outperform the Hapke-HSR model, specifically at two major absorption bands of water (centred at 1.47  
343 and 1.90  $\mu\text{m}$ ), since the HM and MARMIT-2 models fully consider the changes in SSR characteristics with variations in the  
344 SMC. The MRE trends of the three models are basically similar to the RMSE trends, and the HM model demonstrates the  
345 highest level of accuracy, with the MARMIT-2 model following closely behind. The MRE value of the Hapke-HSR model is  
346 approximately 60% at the major absorption band of water (centred at 1.90  $\mu\text{m}$ ), which is significantly greater than that of the  
347 MARMIT-2 model (28%) and the HM model (15%). The bias values of the HM model approach 0.4–2.5  $\mu\text{m}$ , whereas those  
348 of the Hapke-HSR model exhibit a large range of variation. These studies indicate that the HM model results are more in line  
349 with the fitted SSR, whereas the Hapke-HSR model results are more different from the measured SSR values. In general, the  
350 variations between the outputs of these three models and the measured values are in the wavelength ranges of 0.4–0.6  $\mu\text{m}$   
351 and 2.4–2.5  $\mu\text{m}$  and represent the two major absorption bands of water. The soil reflectance is low over the spectral region  
352 from 0.4–0.6  $\mu\text{m}$ , and the soil reflectance variation remains insignificant in this wavelength range as the SMC increases. The  
353 soil measurements have great uncertainty in the range of 2.4–2.5  $\mu\text{m}$ , resulting in poor correlations between the fitting results  
354 of these three models and the measured values. The SSR changes rapidly in the strong absorption band of water, which leads  
355 to great uncertainty in the fitting results of these models. Compared with the observed SSR model, the Hapke-HSR model  
356 has the lowest accuracy, followed by the MARMIT-2 model. The HM and MARMIT-2 models are better than the Hapke-  
357 HSR model at  $\text{SMC} \geq 30\%$  because these two models fully consider the variation in SSR characteristics with the variation in  
358 SMC.

359

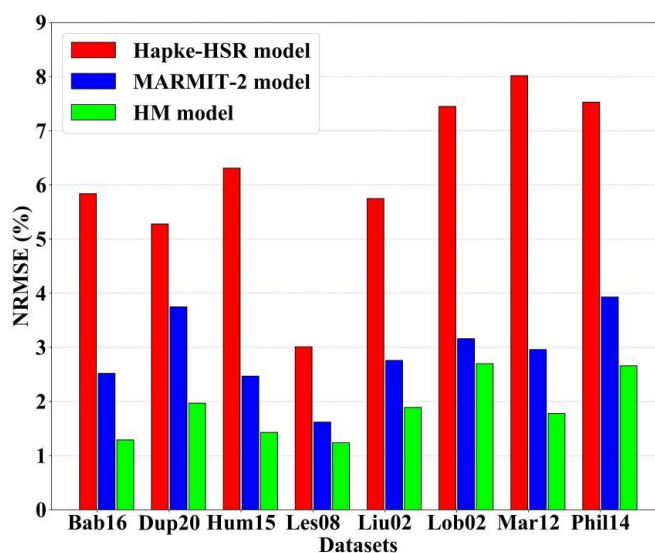


360



361 **Figure 8. Evaluation of the Hapke-HSR (red), MARMIT-2 (blue) and Hapke-HSR + MARMIT-2 (HM) (lime) models**  
 362 **in fitting measured soil reflectance at SMC  $\geq 30\%$ . The assessment indices are the  $R^2$  (a), RMSE (b), MRE (c), and**  
 363 **bias (d) values.**

364 Finally, we analysed the relevant fitting effects of the Hapke-HSR, MARMIT-2, and HM models on eight different  
 365 databases, as shown in Figure 9. These three models exhibit high accuracy (i.e., NRMSE  $< 9\%$ ), whereas the HM and  
 366 MARMIT-2 models notably outperform the Hapke-HSR model in terms of accuracy. For the Bab16, Dup20, Hum15, Liu02,  
 367 Mar12, and Phil14 databases, the accuracy of the measured SSR fit by the HM model is better than that of the Hapke-HSR  
 368 and MARMIT-2 models. The overall NRMSE values decreased by approximately 1.0% (4.3%) compared with those of the  
 369 MARMIT-2 model (Hapke-HSR model). The outcomes of the HM model are substantially better than those of the  
 370 MARMIT-2 model (Hapke-HSR model) for the Dup20 (Mar12) database, and the NRMSE decreases by approximately  
 371 1.8% (6.2%) compared with that of the MARMIT-2 model (Hapke-HSR model). However, the improvement in the HM  
 372 model fitting of the measured observations is small for the Les08 and Lob02 datasets. The main reason is that the MARMIT-  
 373 2 model demonstrates high accuracy for the Les08 database, so the improvement in the HM model is small for this database,  
 374 and the SSR is low for the Lob02 database, resulting in large NRMSE values. In general, the Hapke-HSR, MARMIT-2 and  
 375 HM models show high accuracy in fitting eight different databases, whereas the HM model has an obvious improvement in  
 376 accuracy compared with the MARMIT-2 and Hapke-HSR models.



377  
 378 **Figure 9: The NRMSE values of the measured soil reflectance fit with the Hapke-HSR (red), MARMIT-2 (blue) and**  
 379 **Hapke-HSR + MARMIT-2 (HM) (lime) models for eight different databases.**

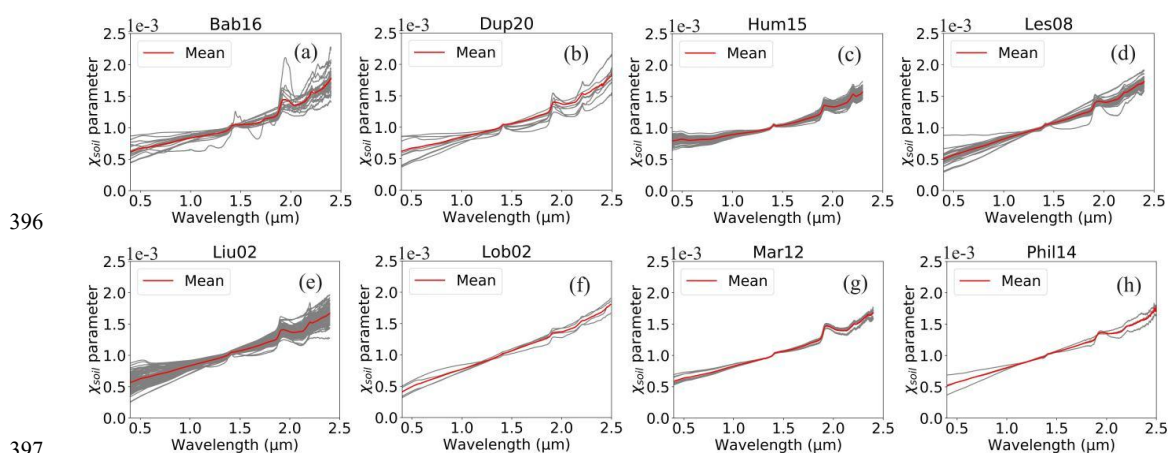
## 380 5 Discussion

### 381 5.1 Analysis of the variation in the parameter $\chi_{soil}$

382 In this section, we analyse the imaginary component of the soil index ( $\chi_{soil}$  parameter) calculated from the dry soil reflectance  
 383 for eight different databases with the wavelengths shown in Figure 10. For different soil databases, the change trend of the  
 384  $\chi_{soil}$  parameter is basically the same. The  $\chi_{soil}$  parameter increases with wavelength, and there is an obvious peak at the two  
 385 strong absorption bands of water (i.e., centred at 1.47 and 1.90  $\mu\text{m}$ ). However, there are still some differences between  
 386 different soil databases. The values of the parameter  $\chi_{soil}$  are greater in the strong absorption band of water for the Bab16 and  
 387 Liu02 databases, whereas the parameter values  $\chi_{soil}$  are lower for the Hum15, Lob02 and Phil14 databases in the strong



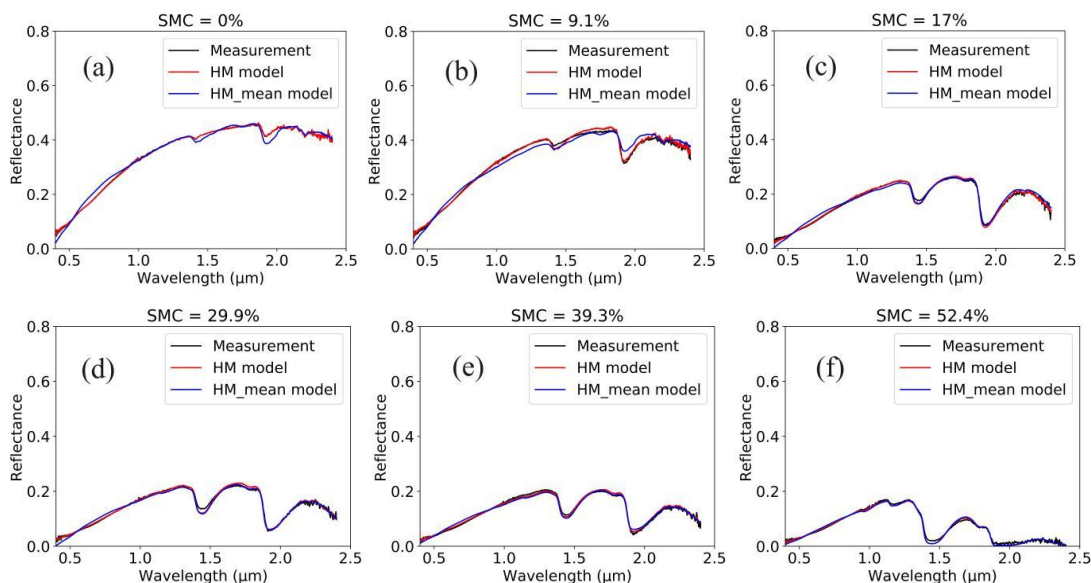
388 absorption band of water; moreover, the influence of the SMC on these three databases is small. For the same soil database,  
 389 the change in the parameter  $\chi_{soil}$  is small, and only the difference between the Bab16 database results is large. In addition, the  
 390 parameter  $\chi_{soil}$  is obviously greater in the two water absorption bands, and the overall change range also decreases. This  
 391 decrease may further affect the accuracy of fitting the measured SSR. Therefore, the method of determining the parameter  
 392  $\chi_{soil}$  in each soil database should be theoretically feasible. The parameter  $\chi_{soil}$  is calculated on the basis of the assumption that  
 393 the dry SSR is similar in shape to the SSA. Therefore, this method still depends on dry soil reflectance, but dry SSR data are  
 394 usually difficult to obtain via field measurements and satellite observations. How to provide a representative dry SSR will be  
 395 our next research focus.



397  
 398 **Figure 10: Analysis of the imaginary component of the soil index (parameter  $\chi_{soil}$ ) for eight different databases (i.e.,**  
 399 **Bab16 (a), Dup20 (b), Hum15 (c), Les08 (d), Liu02 (e), Lob02 (f), Mar12 (g), and Phil14 (h)) with wavelengths.**

### 400 5.2 Validating the Hapke-HSR + MARMIT-2 model using the average parameter $\chi_{soil}$

401 We used the average parameter  $\chi_{soil}$  (i.e., Figure 10(a)) to validate the HM model to characterize the SSR attributes; this  
 402 model is called the HM\_mean model in the following section. Figure 11 shows that the HM and HM\_mean models fit the  
 403 influence of the typical measured SSR value (i.e., bab16\_056-051) at SMC = 0%, 9.1%, 17%, 29.9%, 39.3%, and 52.4%,  
 404 respectively. This set of typical data is thought to have a specular reflection effect when SMC = 52.4%. The HM and  
 405 HM\_mean models match well with the typical measured SSR values. However, the HM model shows greater consistency  
 406 with the fitted SSR value than does the HM\_mean model, especially at SMC < 10%. The HM\_mean model results in  
 407 significant underestimation and overestimation at SMC = 0% and 9.1%, respectively, because the average parameter  $\chi_{soil}$  is  
 408 obviously greater in the water absorption band (Figure 10(a)), which further affects the accuracy of the HM\_mean model.  
 409 The HM and HM\_mean model fitting results can capture the change in SSR with increasing SMC and are highly in line with  
 410 the measured SSR values at high SMCs, which may be caused by the obvious SSR broadening in the strong absorption band  
 411 of water with increasing SMC. In general, the HM model, which uses the average parameter  $\chi_{soil}$ , can still effectively  
 412 describe the SSR characteristics, especially at high SMCs. However, the average parameter  $\chi_{soil}$  leads to a significant  
 413 broadening of the strong absorption band of water at low SMCs, which further leads to obvious overestimation or  
 414 underestimation of the SSR fitted by the HM\_mean model in the strong absorption band of water.



415

416

417 **Figure 11: The HM (red) and HM\_mean (blue) models fit the measured soil reflectance (black) at SMC = 0% (a),**  
 418 **9.1% (b), 17% (c), 29.9% (d), 39.3% (e), and 52.4% (f).**

419 **Table 6.** The HM and HM\_mean models fit the soil reflectance variables and statistical outputs.

Models	SMC	$b$	$M$	$\delta$	$L$	$\epsilon$	$R^2$	RMSE	bias
HM model	0.0	2.0	0.30	0.00	0.00	0.0	1.000	0.001	0.000
	9.1	3.6	0.22	0.14	0.01	0.2	0.996	0.007	0.003
	17.0	1.8	0.32	0.05	0.01	0.6	0.993	0.006	0.000
	29.9	2.2	0.28	0.07	0.02	0.6	0.990	0.006	0.001
	39.3	1.2	0.38	0.06	0.02	0.6	0.990	0.006	0.001
	52.4	1.8	0.32	0.01	0.05	0.9	0.991	0.005	-0.002
	All	--	--	--	--	--	0.998	0.005	0.001
HM_mean model	0.0	2.2	0.18	0.04	0.00	0.9	0.989	0.012	0.001
	9.1	2.2	0.18	0.14	0.00	1.0	0.977	0.016	-0.001
	17.0	0.6	0.34	0.13	0.01	0.6	0.980	0.009	0.002
	29.9	0.6	0.34	0.09	0.02	0.6	0.981	0.008	-0.001
	39.3	1.0	0.26	0.10	0.03	0.6	0.981	0.008	0.000
	52.4	2.6	0.16	0.03	0.06	0.9	0.988	0.006	-0.002
	All	--	--	--	--	--	0.993	0.011	0.000

420

421 Table 6 shows that the HM and HM\_mean models fit the SSR parameters and statistical outputs. The overall accuracy  
 422 of the HM and HM\_mean models in terms of fitting the measured SSR is high ( $R^2 = 0.991-0.993$ ,  $RMSE = 0.005-0.011$ ).  
 423 According to the simulation results, the HM model is more accurate with respect to the measured SSR than the HM\_mean  
 424 model is, especially at  $SMC < 10\%$ , because the average parameter  $\chi_{soil}$  is obviously greater in the water absorption band.  
 425 The HM and HM\_mean models can effectively describe SSR features, especially high SMCs ( $R^2 > 0.98$  and  $RMSE < 0.01$ ).  
 426 When  $SMC = 52.4\%$ , the measured soil spectral data are suspected to have a specular reflection effect, and the HM model



427 maintains a higher fitting accuracy ( $R^2 = 0.991$ ,  $RMSE = 0.005$ ) than does the Hapke\_mean model ( $R^2 = 0.988$ ,  $RMSE =$   
 428  $0.006$ ). These results indicate that the method of assuming an average parameter  $\chi_{soil}$  in each soil database should be  
 429 theoretically feasible. However, all the soil types may have large differences in the parameter  $\chi_{soil}$ . How to select the  
 430 parameter  $\chi_{soil}$  of each soil type will be particularly important in our subsequent study.

431 Finally, we calculate the overall average parameter  $\chi_{soil}$  to determine the dependence of the HM model on the dry SSR.  
 432 First, we normalize all  $\chi_{soil}$  parameters to the same order of magnitude and then average these indices in each band. Finally,  
 433 we use all the SSR data to verify the accuracy of this method. Table 7 shows that the HM\_mean model fit the statistical  
 434 results for all the SSR data. Compared with the measured SSR, the HM\_mean model has high fitting accuracy. The  $R^2$  value  
 435 of the HM\_mean model is 0.988, and the RMSE is 0.014, indicating negligible bias. However, the fitting accuracy of the  
 436 overall SSR data of the HM\_mean model is lower than that of the MARMIT-2 and HM models (i.e., Figure 6(b)-(c)). The  
 437 main reason is that there are notable discrepancies in the parameter  $\chi_{soil}$  among various soil types (Figure 10). The model  
 438 operation can be simplified by averaging all the  $\chi_{soil}$  parameters of the soil, but this approach also results in an accuracy  
 439 decline for the HM\_mean model. For SMC values  $\geq 30\%$ , the HM\_mean model results in a lower RMSE than that for SMC  
 440 values  $< 30\%$ , which is consistent with the findings illustrated in Figure 11 and Table 6. However, the NRMSE and MRE  
 441 values of the HM\_mean model at  $SMC \geq 30\%$  were lower than those at  $SMC < 30\%$ , possibly because the dry SSR is  
 442 greater than that of wet soil. In conclusion, the HM\_mean model demonstrates proficiency in describing SSR attributes, and  
 443 the overall average parameter  $\chi_{soil}$  of the soil can be used to determine the dependence of the HM model on the SSR. In this  
 444 study, we based our analysis solely on the soil databases, which has limitations. In future research, we will consider soil  
 445 properties or spectrally similar soils and account for more factors affecting the  $\chi_{soil}$  parameter to improve the accuracy of the  
 446 Hapke-HSR + MARMIT-2 model.

447 **Table 7.** The HM\_mean model fit the statistical results for all the soil reflectance data.

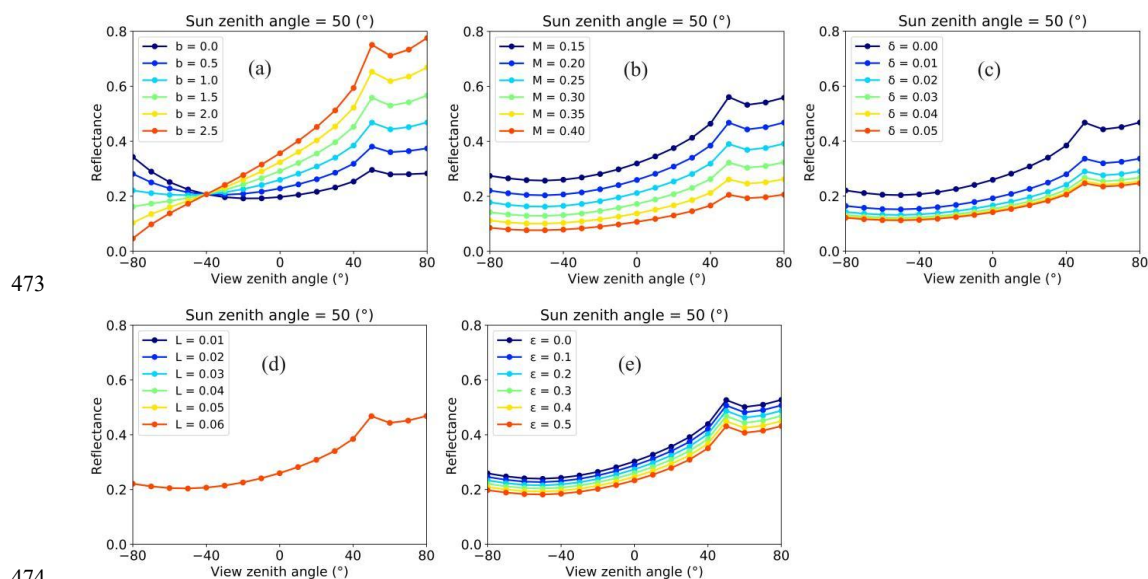
Data	Number	$R^2$	RMSE	NRMSE (%)	MRE (%)	bias
SMC $< 30\%$	2257585	0.989	0.015	1.811	5.117	0.000
SMC $\geq 30\%$	1082887	0.980	0.013	1.858	6.988	0.000
All	3340472	0.988	0.014	1.743	5.723	0.000

### 448 5.3 Analysing the Parameter Influence of the Hapke-HSR + MARMIT-2 model on the soil BRDF shape

449 Finally, we analyse the impact of the soil parameters on the BRDF shape obtained with the Hapke-HSR + MARMIT-2  
 450 model. Considering that we previously used various BRDF data sources to examine the role of the Hapke-HSR model in  
 451 modelling soil BRDF features, we analyse how the model parameters affect the shape of the BRDF curve (Ding et al., 2022).  
 452 Figure 12 shows the effects of parameters  $b$ ,  $M$ ,  $\delta$ ,  $L$  and  $\epsilon$  in the Hapke-HSR + MARMIT-2 (HM) model on the soil BRDF  
 453 shape in the principal plane (PP). With increasing parameter  $b$ , the soil reflectance gradually decreases in the forwards  
 454 direction but increases in the backwards reflection direction. The parameter  $b$  has a relatively large contribution to the  
 455 anisotropy characteristics of the soil. When the parameter  $M$  increases, the soil reflectance continuously decreases. The soil  
 456 anisotropy is strongest when the parameter  $M$  is relatively small. With the increase in the parameter  $\delta$ , the impact of the  
 457 parameter  $\delta$  on the soil reflectance is relatively large in the range of 0-0.01, and the anisotropy of the soil is strong; however,  
 458 the influence of the parameter  $\delta$  on the SSR is relatively low, and the soil anisotropy is significantly weak. As the parameter  
 459  $L$  increases,  $L$  does not impact the soil reflectance, which corresponds with the results in Figure 3(g). With increasing value  
 460 of the parameter  $\epsilon$ , the equal interval of the soil reflectance decreases since the influence of the surface coverage fraction of  
 461 water is proportionally related to this factor. In summary, the variation in the parameters  $b$  and  $M$  in the Hapke-HSR model  
 462 has a notable effect on the soil BRDF shape, whereas the parameters of the MARMIT-2 model have a relatively minimal  
 463 effect on the soil BRDF shape. Therefore, the ability of the HM model to describe the features of the soil BRDF is basically  
 464 consistent with that of the Hapke-HSR model. This occurs because the MARMIT-2 model does not include additional



465 BRDF-related information, whereas the Hapke-HSR model includes input parameters for angle-related information. In future  
 466 studies, we will comprehensively assess the ability of the HM model to represent soil BRDF features, especially in the  
 467 forwards direction for wet soil. In addition, our study has certain limitations, such as ignoring the effects of certain  
 468 parameters, namely, surface roughness and porosity, on the soil reflectance characteristics to simplify the analysis. The  
 469 rationale for this approach is that our primary focus was on coupling the improved Hapke-HSR model with the MARMIT-2  
 470 model to characterize the spectral reflectance of dry and wet soils. The validation results show that despite neglecting several  
 471 factors, our proposed coupling method still demonstrates high accuracy, indicating that the method presented in this paper is  
 472 suitable for representing soil reflectance characteristics.



473  
 474  
 475 **Figure 12: Influence of the coefficient of  $b$  (a), soil particle size and shape-dependent  $M$  (b), volume fraction  $\delta$  (c),**  
 476 **thickness  $L$  (d) and surface coverage fraction of water  $\epsilon$  (e) parameters of the Hapke-HSR + MARMIT-2 (HM) model**  
 477 **on the soil BRDF shape in the red band ( $0.67 \mu\text{m}$ ).**

## 478 6 Conclusion

479 This study develops a unified soil radiative transfer framework by refining the improved Hapke-HSR model and dynamically  
 480 coupling it with the MARMIT-2 model to improve the representation of soil reflectance under varying soil moisture  
 481 conditions. The primary objective is to overcome the limitations of the Hapke-HSR model in wet soils and the dependence of  
 482 MARMIT-2 model on externally prescribed dry reflectance, thereby extending the applicability of both models.

483 First, dry SSR is used to estimate the imaginary part of the soil refractive index ( $\chi_{\text{soil}}$ ), which alleviates the piecewise  
 484 fitting limitation of the Hapke-HSR model by establishing a continuous statistical relationship between single scattering  
 485 albedo and wavelength. The improved Hapke-HSR is then coupled with MARMIT-2 to integrate particle scattering and  
 486 moisture-dependent absorption processes within a physically consistent framework. The proposed Hapke-HSR + MARMIT-  
 487 2 (HM) model is evaluated using multiple independent soil spectral databases. The results show that all three models  
 488 reproduce measured SSR with reasonable accuracy, whereas the coupled HM model achieves consistently higher  
 489 performance ( $R^2 = 0.993$ ,  $\text{RMSE} = 0.007$ ) than MARMIT-2 ( $R^2 = 0.983$ ,  $\text{RMSE} = 0.012$ ) and Hapke-HSR ( $R^2 = 0.909$ ,  
 490  $\text{RMSE} = 0.028$ ), with particularly pronounced improvements at high soil moisture levels ( $\text{SMC} \geq 30\%$ ). This study does not  
 491 aim to replace the MARMIT-2 model, which already provides an effective description of moisture effects, but rather to



492 improve the overall physical consistency of soil reflectance modeling through the integration of complementary mechanisms.  
 493 The coupled framework provides a robust basis for future developments in soil parameter inversion, particularly for soil  
 494 moisture, and for improved representation of soil background effects in land-surface radiative transfer modeling.

495 In summary, this work addresses two key modeling challenges: (1) improving the hyperspectral consistency of the  
 496 Hapke-HSR using dry soil reflectance, and (2) establishing a unified coupling strategy that jointly represents spectral  
 497 behavior and moisture-dependent effects. The proposed framework contributes to the theoretical and methodological  
 498 foundation of soil radiative transfer modeling and supports future advances in optical remote sensing of land-surface  
 499 parameters.

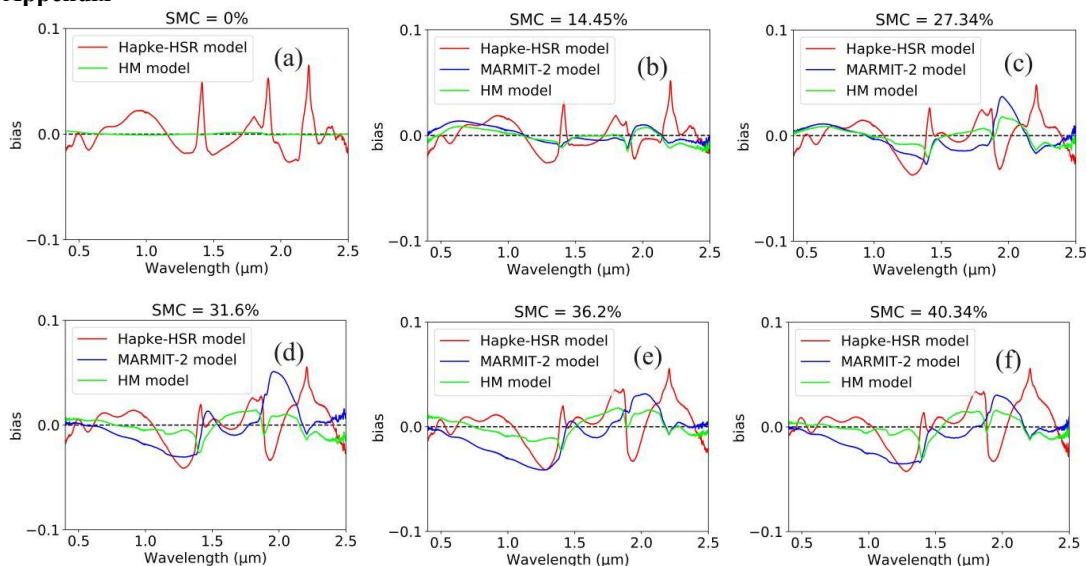
500 *Code and data availability.* The Hapke-HSR + MARMIT-2 model code and example datasets used in this study are archived  
 501 on Zenodo (<https://doi.org/10.5281/zenodo.18366791>; Ding, 2025). The original soil databases are derived from the  
 502 MARMIT framework (<https://pss-gitlab.math.univ-paris-diderot.fr/marmit/marmit>).

503 *Author contributions.* Conceptualization, Anxin Ding, Shunlin Liang; methodology, Anxin Ding, Han Ma, Shunlin Liang,  
 504 Ziti Jiao and Alexander A.Kokhanovsky; formal analysis, Anxin Ding, Han Ma and Rui Xie; data curation, Han Ma, Ziti  
 505 Jiao and Rui Xie; software, Han Ma; investigation, Ziti Jiao; theoretical support, Alexander A.Kokhanovsky; data processing  
 506 and validation, Hanyu Shi; supervision, Shunlin Liang; writing—original draft, Anxin Ding; writing—review and editing,  
 507 Han Ma, Shunlin Liang, Ziti Jiao, Hanyu Shi, Alexander A.Kokhanovsky and Rui Xie.

508 *Competing interests.* The authors have no conflict of interest.

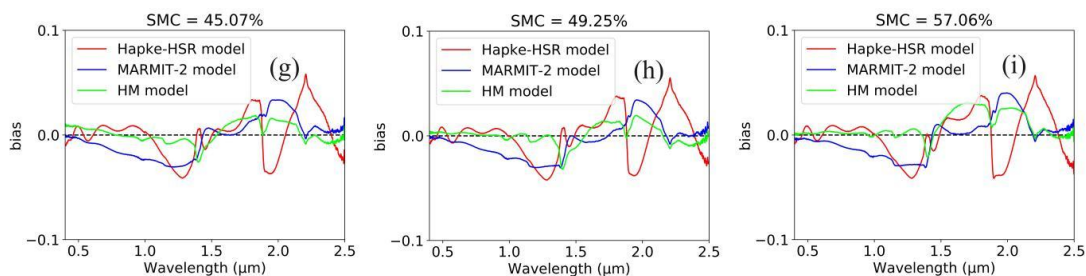
509 *Acknowledgments.* This study was supported by the National Natural Science Foundation of China (Grant No. 42301363)  
 510 and the Anhui Province Youth Science and Technology Talent Lift Program (Grant No. RCTJ202404). We gratefully  
 511 acknowledge Stéphane Jacquemoud and his team for sharing the implementation of the MARMIT-2 model, which provided  
 512 valuable support for this study.

513 **Appendix**



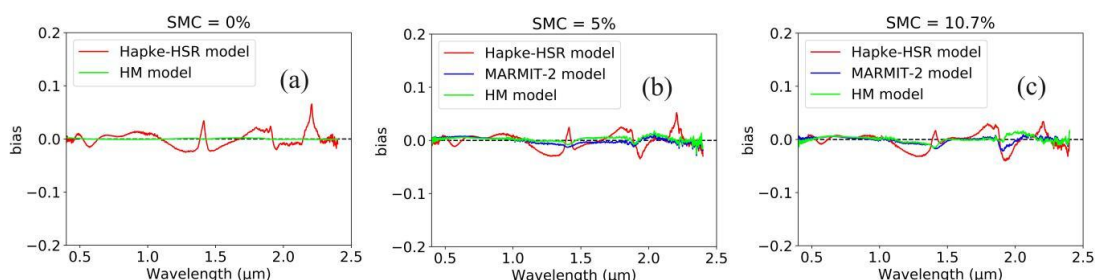
514

515

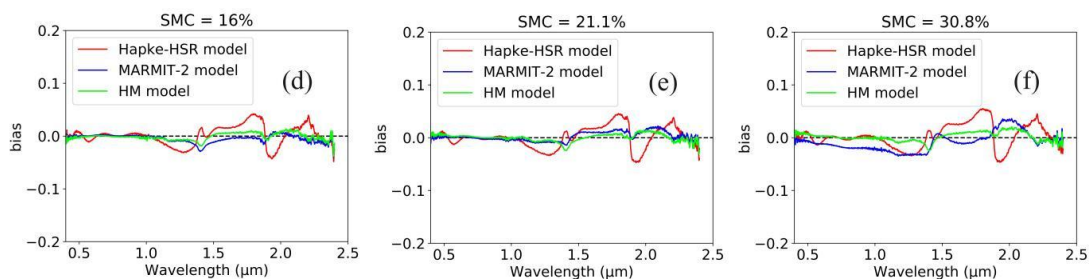


516

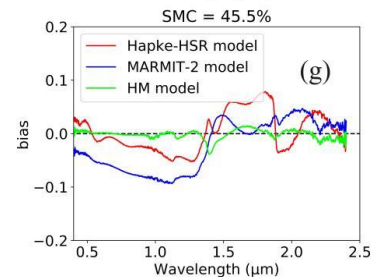
517 **Figure A1: The bias (i.e., simulated reflectance of these models - measured reflectance) between the simulated**  
 518 **spectral reflectance of the Hapke-HSR (red), MARMIT-2 (blue) and Hapke-HSR + MARMIT-2 (HM) (lime) models**  
 519 **and the fitted soil reflectance at SMC = 0% (a), 14.45% (b), 27.34% (c), 31.6% (d), 36.2% (e), 40.34% (f), 45.07% (g),**  
 520 **49.25% (h), and 57.06% (i).**



521



522



523

524 **Figure A2. The bias (i.e., simulated reflectance of these models - measured reflectance) between the simulated**  
 525 **reflectance of the Hapke-HSR (red), MARMIT-2 (blue) and Hapke-HSR + MARMIT-2 (HM) (lime) models and the**  
 526 **fitted soil reflectance at SMC = 0% (a), 5% (b), 10.7% (c), 16% (d), 21.1% (e), 30.8% (f), and 45.5% (g).**

527

528

529



530 **References**

- 531 Ångström, A.: The albedo of various surfaces of ground, *Geografiska Annaler Series A: Physical Geography*, 7, 323–342,  
532 1925.
- 533 Babelt, A., Vu, P. V. H., Jacquemoud, S., Viallefont-Robinet, F., Fabre, S., Briottet, X., Sadeghi, M., Whiting, M. L., Baret,  
534 F., and Tian, J.: MARMIT: a multilayer radiative transfer model of soil reflectance to estimate surface SMC in the solar  
535 domain 400–2500 nm, *Remote Sensing of Environment*, 217, 1–17, 2018.
- 536 Bach, H. and Mauser, W.: Modeling and model verification of the spectral reflectance of soils under varying moisture  
537 conditions, *IGARSS*, 4, 2354–2356, 1994.
- 538 Cheng, J., Wen, J., Xiao, Q., Wu, S., Hao, D., and Liu, Q.: Extending the GOSAILT model to simulate sparse woodland  
539 bidirectional reflectance with soil reflectance anisotropy consideration, *Remote Sensing*, 14, 1001, 2022.
- 540 Ding, A., Ma, H., Liang, S., and He, T.: Extension of the Hapke model to the spectral domain to characterize soil physical  
541 properties, *Remote Sensing of Environment*, 269, 112843, 2022.
- 542 Ding, A.: Hapke-HSR + MARMIT-2 soil radiative transfer model, *Zenodo*, <https://doi.org/10.5281/zenodo.18366791>, 2025.
- 543 Dupiau, A., Jacquemoud, S., Briottet, X., Fabre, S., Viallefont-Robinet, F., Philpot, W., Di Biagio, C., Hébert, M., and  
544 Formenti, P.: MARMIT-2: an improved version of the MARMIT model to predict soil reflectance as a function of surface  
545 water content in the solar domain, *Remote Sensing of Environment*, 272, 112951, 2022.
- 546 Fan, D., Zhao, T., Jiang, X., García-García, A., Schmidt, T., Samaniego, L., Attinger, S., Wu, H., Jiang, Y., Shi, J., Fan, L.,  
547 Tang, B. H., Wagner, W., Dorigo, W., Gruber, A., Mattia, F., Balenzano, A., Brocca, L., Jagdhuber, T., Wigneron, J. P.,  
548 Montzka, C., and Peng, J.: A Sentinel-1 SAR-based global 1 km resolution soil moisture data product: algorithm and  
549 preliminary assessment, *Remote Sensing of Environment*, 318, 114579, 2025.
- 550 Gao, S., Yan, K., Liu, J., Pu, J., Zou, D., Qi, J., and Yan, G.: Assessment of remote-sensed vegetation indices for estimating  
551 forest chlorophyll concentration, *Ecological Indicators*, 162, 112001, 2024.
- 552 Gholami, B. N. and Mobasheri, M. R.: Influence of soil texture on the estimation of bare soil moisture content using MODIS  
553 images, *European Journal of Remote Sensing*, 51, 911–920, 2018.
- 554 Hapke, B.: Bidirectional reflectance spectroscopy 7: the single particle phase function hockey stick relation, *Icarus*, 221,  
555 1079–1083, 2012.
- 556 Jacquemoud, S.: Modeling spectral and bidirectional soil reflectance, *Remote Sensing of Environment*, 41, 123–132, 1992.
- 557 Jiang, C. and Fang, H.: GSV: a general model for hyperspectral soil reflectance simulation, *Int. J. Appl. Earth Obs. Geoinf.*,  
558 83, 101932, 2019.
- 559 Jiang, H., Wei, X., Chen, Z., Zhu, M., Yao, Y., Zhang, X., and Jia, K.: Influence of different soil reflectance schemes on the  
560 retrieval of vegetation LAI and FVC from PROSAIL in agricultural regions, *Comput. Electron. Agric.*, 12, 108165, 2023.
- 561 Kimmel, B. W. and Baranoski, G. V. G.: A novel approach for simulating light interaction with particulate materials:  
562 application to the modeling of sand spectral properties, *Opt. Express*, 15, 9755–9777, 2007.
- 563 Labarre, S., Jacquemoud, S., Ferrari, C., Delorme, A., Derrien, A., Grandin, R., Jalludin, M., Lemaitre, F., Métois, M.,  
564 Pierrot-Deseilligny, M., Rupnik, E., and Tanguy, B.: Retrieving soil surface roughness with the Hapke photometric model:  
565 confrontation with the ground truth, *Remote Sens. Environ.*, 225, 1–15, 2019.
- 566 Lekner, J. and Dorf, M. C.: Why some things are darker when wet, *Appl. Opt.*, 27, 1278–1280, 1988.
- 567 Lei, T. and Bailey, B. N.: A text-based generative deep learning model for soil reflectance spectrum simulation in the solar  
568 range (400–2499 nm), *Remote Sens. Environ.*, 318, 114527, 2025.
- 569 Li, L., Mu, X., Qi, J., Pisek, J., Roosjen, P., Yan, G., Huang, H., Liu, S., and Baret, F.: Characterizing reflectance anisotropy  
570 of background soil in open-canopy plantations using UAV-based multiangular images, *ISPRS J. Photogramm. Remote Sens.*,  
571 177, 263–278, 2021.



- 572 Liang, S. and Townshend, J. R. G.: A parametric soil BRDF model: a four-stream approximation for multiple scattering, *Int.*  
573 *J. Remote Sens.*, 17, 1303–1315, 1996.
- 574 Liang, S. and Townshend, J. R. G.: A modified Hapke model for soil bidirectional reflectance, *Remote Sens. Environ.*, 55,  
575 1–10, 1996.
- 576 Ma, H., Liang, S., Xiao, Z., and Shi, H.: Simultaneous inversion of multiple land surface parameters from MODIS optical-  
577 thermal observations, *ISPRS J. Photogramm. Remote Sens.*, 128, 240–254, 2017.
- 578 Ma, H., Liu, Q., Liang, S., and Xiao, Z.: Simultaneous estimation of leaf area index, fraction of absorbed photosynthetically  
579 active radiation, and surface albedo from multiple-satellite data, *IEEE Trans. Geosci. Remote Sens.*, 55, 4334–4354, 2017.
- 580 Ni, W. and Li, X.: A coupled vegetation–soil bidirectional reflectance model for a semiarid landscape, *Remote Sens.*  
581 *Environ.*, 74, 113–124, 2000.
- 582 Nolin, A. W. and Liang, S.: Progress in bidirectional reflectance modeling and applications for surface particulate media:  
583 snow and soils, *Remote Sens. Rev.*, 18, 307–342, 2000.
- 584 Rizzo, R., Wadoux, A. M. J.-C., Demattê, J. A. M., Minasny, B., Barrón, V., Ben-Dor, E., Francos, N., Savin, I., Poppiel, R.,  
585 Silvero, N. E. Q., Terra, F. S., Rosin, N. A., Rosas, J. T. F., Greschuk, L. T., Ballester, M. R. V., Gómez, A. M. R.,  
586 Bellinaso, H., Safanelli, J. L., Chabrillat, S., Fiorio, P. R., Das, B. S., Malone, B. P., Zalidis, G., Tziolas, N., Tsakiridis, N.,  
587 Karyotis, K., Samarinas, N., Kalopesa, E., Gholizadeh, A., Shepherd, K. D., Milewski, R., Vaudour, E., Wang, C., and  
588 Salama, E. S. M.: Remote sensing of the Earth’s soil color in space and time, *Remote Sens. Environ.*, 299, 113845, 2023.
- 589 Sadeghi, M., Babaeian, E., Tuller, M., and Jones, S. B.: The optical trapezoid model: a novel approach to remote sensing of  
590 soil moisture applied to Sentinel-2 and Landsat-8 observations, *Remote Sens. Environ.*, 198, 52–68, 2017.
- 591 Sadeghi, M., Jones, S. B., and Philpot, W. D.: A linear physically based model for remote sensing of soil moisture using  
592 shortwave infrared bands, *Remote Sens. Environ.*, 164, 66–76, 2015.
- 593 Sheng, Y., Sun, Z., Lu, S., and Omasa, K.: Ratio of physical model parameters can retrieve aggregate size from different  
594 types of soil in cultivated regions, *Soil Tillage Res.*, 244, 106262, 2024.
- 595 Shoshany, M., Roitberg, E., Goldshleger, N., and Kizel, F.: Universal quadratic soil spectral reflectance line and its deviation  
596 patterns’ relationships with chemical and textural properties: a global database analysis, *Remote Sens. Environ.*, 155, 198–  
597 230, 2022.
- 598 Verhoef, W., Van der Tol, C., and Middleton, E. M.: Hyperspectral radiative transfer modeling to explore the combined  
599 retrieval of biophysical parameters and canopy fluorescence from FLEX–Sentinel-3 tandem mission multi-sensor data,  
600 *Remote Sens. Environ.*, 204, 942–963, 2018.
- 601 Verhoef, W. and Bach, H.: Coupled soil–leaf–canopy and atmosphere radiative transfer modeling to simulate hyperspectral  
602 multi-angular surface reflectance and TOA radiance data, *Remote Sens. Environ.*, 109, 166–182, 2007.
- 603 Xu, H., Sun, H., Xu, Z., Wang, Y., Zhang, T., Wu, D., and Gao, J.: kNDMI: a kernel normalized difference moisture index  
604 for remote sensing of soil and vegetation moisture, *Remote Sens. Environ.*, 319, 114621, 2025.
- 605 Yang, G. J., Zhao, C. J., Huang, W. J., and Wang, J. H.: Extension of the Hapke bidirectional reflectance model to retrieve  
606 soil water content, *Hydrol. Earth Syst. Sci.*, 15, 2317–2326, 2011.
- 607 Yang, P.: Exploring the interrelated effects of soil background, canopy structure, and sun–observer geometry on canopy  
608 photochemical reflectance index, *Remote Sens. Environ.*, 279, 113133, 2022.
- 609 Yang, P., van der Tol, C., Liu, J., and Liu, Z.: Separation of the direct reflection of soil from canopy spectral reflectance,  
610 *Remote Sens. Environ.*, 316, 114500, 2025.
- 611 Zeng, Y., Hao, D., Badgley, G., Damm, A., Rascher, U., Ryu, Y., Johnson, J., Krieger, V., Wu, S., Qiu, H., Liu, Y., Berry, J.  
612 A., and Chen, M.: Estimating near-infrared reflectance of vegetation from hyperspectral data, *Remote Sens. Environ.*, 267,  
613 112723, 2021.

<https://doi.org/10.5194/egusphere-2026-344>

Preprint. Discussion started: 3 March 2026

© Author(s) 2026. CC BY 4.0 License.



614 Zhao, X., Qi, J., Xu, H., Yu, Z., Yuan, L., Chen, Y., and Huang, H.: Evaluating the potential of airborne hyperspectral  
615 LiDAR for assessing forest insects and diseases with 3D radiative transfer modeling, *Remote Sens. Environ.*, 297, 113759,  
616 2023.